CONTROLLER DESIGN FOR ACCURATE

ANTENNA POINTING ONBOARD A SPACECRAFT

THESIS

Victor M. Barba, Ensign, USN

AFIT/GAE/ENG/07-03

DEPARTMENT OF THE AIR FORCE
AIR UNIVERSITY
AIR FORCE INSTITUTE OF TECHNOLOGY

Wright-Patterson Air Force Base, Ohio

AFIT/GAE/ENG/07-03

CONTROLLER DESIGN FOR ACCURATE ANTENNA POINTING ONBOARD A SPACECRAFT

THESIS

Presented to the Faculty

Department of Electrical and Computer Engineering

Graduate School of Engineering and Management

Air Force Institute of Technology

Air University

Air Education and Training Command

In Partial Fulfillment of the Requirements for the

Degree of Master of Science in Aeronautical Engineering

Victor M. Barba, BS

Ensign, USN

June 2007

AFIT/GAE/ENG/07-03

CONTROLLER DESIGN FOR ACCURATE ANTENNA POINTING ONBOARD A SPACECRAFT

Victor M. Barba, BS

Ensign, USN

Approved:

//signed//	
Dr. Meir Pachter (Chairman)	date
//signed//	
Major Eric Swenson (Member)	date
//signed//	
Dr. Robert Canfield (Member)	date

Abstract

Controller design for a spacecraft mounted flexible antenna is considered. The antenna plant model has a certain degree of uncertainty. Additionally, disturbances from the host spacecraft are transmitted to the antenna and need to be attenuated. The design concept explored herein entails feedforward control to slew the antenna. Feedback control is then used to compensate for plant uncertainty and to reject the disturbance signals. A tight control loop is designed to meet performance specifications while minimizing the control gains.

Simulations are conducted to show that the integration of feedforward control action and feedback compensation produces better responses than the implementation of either individual control system. Integration results in lower gains and still meets the performance specifications

Critical plant parameters are varied to simulate the uncertainty in the nominal plant. The control system is then exercised on several variations of the nominal plant. A worst case plant is produced as a combination of the variations to the nominal plant. Simulations show that when the controller is implemented on the worst case plant, specifications are exceeded. The controller gains are reduced and the simulations are repeated so that the specifications are met but not exceeded; thus, proving that a reduction of plant uncertainty allows the reduction of the control gains.

Acknowledgments

I would like to express my sincere appreciation to my faculty advisor, Dr. Meir Pachter, for his guidance and support throughout the course of this thesis effort. His insight, knowledge, and experience were greatly appreciated. I would also like to acknowledge Major Eric Swenson for his time to assist me in writing. I would also like to thank my sponsors, Major Eric Nelson and Dr. Richard Witt of the Pentagon, for the opportunity to work on this project.

Finally, none of this would be possible without my family and friends back home and out in the fleet; I could not have done this without them. Their continuous support and encouragement have been phenomenal. Special thanks to my fellow AFIT Navy Ensigns who gave me the camaraderie and support I needed to stay focused throughout my research efforts.

Victor M. Barba

Table of Contents

Page

List of Figures

Page

List of Tables

Page

CONTROLLER DESIGN FOR ACCURATE ANTENNA POINTING ONBOARD A SPACECRAFT

I. Introduction

1.1. Problem Statement

Spacecraft mounted payloads often times require very accurate tracking performance capabilities. For example, a spacecraft mounted flexible antenna requires high accuracy and precision control to perform its mission. The precision and accuracy required to achieve the desired performance typically requires the use of a high gain feedback control system and accurate plant knowledge.

In the case of spacecraft applications, the plant dynamics are often difficult to assess because the zero-gravity environment is not easily replicated on Earth; thus suitable experiments can not be conducted until the spacecraft is launched in orbit. Therefore, the main challenge is the ability to implement a control system on a plant with uncertain parameters.

The Department of Defense and the United States Air Force have taken special interest in the investigation of this common problem inherent in spacecraft payload pointing control.

1.2. Research Focus

The first part of this investigation addresses the control problem for a spacecraft mounted flexible antenna. Because of tight performance specifications, the typical controls approach is to design a feedback controller with high gains. In addition, the plant parameters should be accurate; otherwise, the control system may not be able to

meet the performance specifications. Again, the use of high gain feedback control increases the performance of the system; however, methods of reducing uncertainty in plant parameters can be investigated, which eases the need for high gain feedback control. Classical control theory encourages the use of high gain to increase robustness and disturbance rejection. However, the use of high gains is limited by both actuator saturation and sensor noise amplification.

To demonstrate the limitations of the implementation of high gains consider the feedback control scheme shown in Fig. 1-1. The plant transfer function is represented in block, *P(s)*. The forward loop compensator is $G_c(s)$, and the feedback compensator is *H(s)*. The disturbance signal d_1 is from motor vibrations, the disturbance signal d_2 is from the host spacecraft vibration. The reference signal, θ_r, is typically a step command in classical controls to show that the objective is to slew from one angle to another. The use of high gains is conducive to the rejection of d_1 and d_2, as shown in Equations 1-1 and 1-2. However, the use of high gains is limited by actuator saturation, that is, a motor can only produce so much torque and can only increase/decrease the torque at a certain rate. High gains also amplify the sensitivity to sensor noise, *n*, as shown in Equation 1-3.

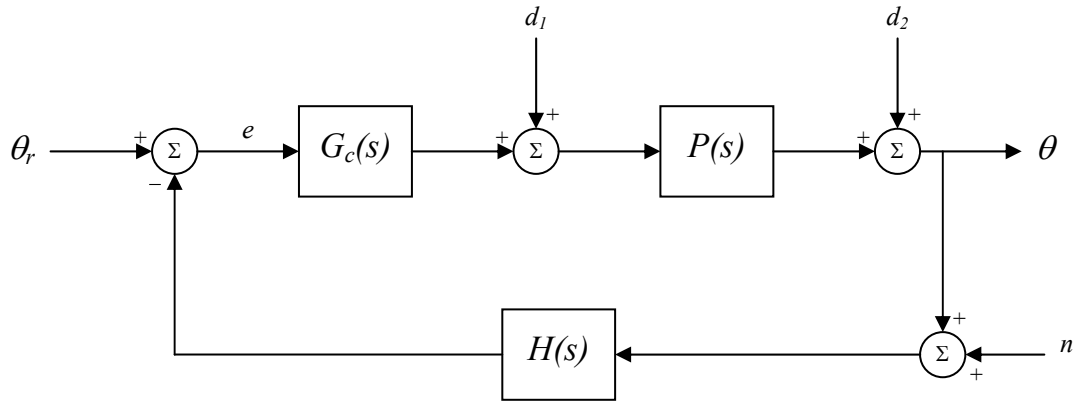

Figure 1-1: Feedback Control System

Equations 1-1 and 1-2 illustrate that the magnitude of the sensitivity transfer functions of d_1 and d_2 are reduced by increasing the gains in $G_c(s)$ and $H(s)$. A lower magnitude of the sensitivity transfer functions is synonymous to a higher rejection of a disturbance signal. To reduce notation, because $S_1(s)$ and $S_2(s)$ behave similarly, only $S_2(s)$ is considered further in this investigation.

$$\left|S_1(j\omega)\right| \triangleq \left|\frac{\theta(j\omega)}{d_1(j\omega)}\right| = \left|\frac{P(s)}{1+P(s)G_c(s)H(s)}\right|_{s=j\omega} \tag{1-1}$$

$$\left|S_2(j\omega)\right| \triangleq \left|\frac{\theta(j\omega)}{d_2(j\omega)}\right| = \left|\frac{1}{1+P(s)G_c(s)H(s)}\right|_{s=j\omega} \tag{1-2}$$

The third sensitivity function is for the sensor disturbance noise (Equation 1-3). A decrease in magnitude of $S_2(s)$ directly results in the increase in magnitude of $S_3(s)$ – herein, is the tradeoff between disturbance rejection and sensor noise amplification. Apart from actuator saturation, the converse relationship between disturbance rejection and noise sensitivity relationship shows that an increase of gains results in a higher sensitivity to sensor noise. Again, since the relationship between S_2 and S_3 remains constant, only S_2 will be considered in this investigation.

$$\left|S_3(j\omega)\right| \triangleq \left|\frac{\theta(j\omega)}{N(j\omega)}\right| = \left|\frac{P(s)G_c(s)H(s)}{1+P(s)G_c(s)H(s)}\right|_{s=j\omega} = \left|1-S_2(j\omega)\right| \tag{1-3}$$

The second part of this investigation addresses the issue of plant uncertainty. Spacecraft dynamics are often difficult to determine on Earth because of the inability to mimic the space environment on Earth. A common solution is to conduct experiments while the spacecraft is in orbit; from these experiments the plant parameters can be determined. This method is commonly referred to as system identification (SYS ID).

SYS ID eliminates most of the environmental uncertainties and it can be occasionally repeated should the plant vary over time. However, the SYS ID methodology itself has experimental uncertainties which are unavoidable. Even the most advanced applications of SYS ID have limited certainty in modeling the plant.

One approach to the uncertainty issue is to identify the error sources of experimental uncertainty. By reducing the plant uncertainty – or at the very least defining certain bounds of uncertainty – the control system can be designed with lower gains since the uncertainty bounds are better defined. Addressing the plant uncertainty is not covered in the scope of this investigation. Rather, the effects of plant uncertainty on the control system response are studied. The importance of bounding the uncertainty in plant parameters is demonstrated.

The important issue in this investigation is the limited capabilities of designing for robustness due to external disturbances and plant uncertainty. The implementation of a feedback controller with high gains is limited by instability, actuator saturation, and noise amplification. The design problem is determining how to achieve tight performance specifications while minimizing the use of high gains.

1.3. Research Objectives

The objective of this research effort is to design a controller which meets given performance specifications given a nominal plant without exclusively relying on the use of high gains. To ease the need for high gains, a feedforward control concept is evaluated. The concept that feedforward control eases the need of high gain feedback compensation is evaluated. In addition, the feedback reference signal, θ_r, is smoothed

from a step response to a continuous curve which slews the structure in a smooth and continuous manner. The reference signal is the expected output of feedback control; therefore, by setting the output of open loop feedforward control equal to the reference input, the error signal to the feedback controller (integrated with feedforward control) is reduced during the slewing maneuver. Additionally, The controller should be designed such that it is robust enough to meet the performance specifications on reasonable variants of the nominal plant.

The plant model is considered to be a spacecraft mounted flexible antenna. The flexible antenna is modeled similar to a torsional spring-mass-damper (SMD) system illustrated in Figure 1-2. The nominal plant and its parameters are presented in Appendix A.

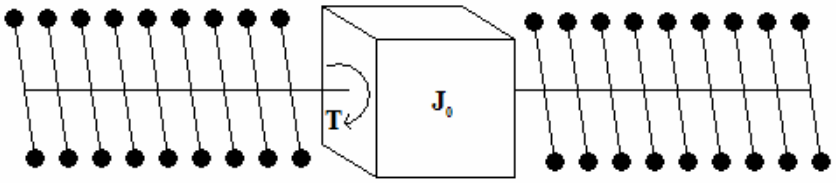

Figure 1-2: Illustration of Flexible Model

Experiments are conducted with the designed tight control loop on variants of the nominal antenna plant model. The variants are created by modifying plant parameters such as flexible mode frequencies, moment of inertia, and time delays. The effects of the uncertainty in the plant are quantitatively defined. Quantities such as disturbance attenuation, tracking error, speed of response, and gain and phase margins are considered as bases of comparison.

The objective is to achieve performance specifications for the "worst case" plant, while also achieving good disturbance effect attenuation when compared to open loop control. The control design methodology is inspired by the Quantitative Feedback Theory (QFT) control design method (D'Azzo and Houpis, 1995).

1.4. Methodology

The implemented feedforward control slews the antenna from one angle to another. The slewing maneuver is completed without the aid of the feedback control. Since the nominal plant is known, a nominal open loop response can be achieved with feedforward control. The use of feedforward control allows the gains of the feedback controller to remain low, since the responsibility of slewing the antenna is given primarily to the feedforward control. To further reduce the impact of the feedback controller on slewing, the reference signal, θ_r, is modified from a classical discontinuous step to match the desired open loop response. Ideally, this reference signal gives a zero error signal to the feedback compensator for the duration of the slewing maneuver. However, since the plant is not fully known, flexible body modes may be excited in the structure, resulting in unwanted vibrations during the feedforward control process. These vibrations will cause an error between the reference signal and the actual response, thus triggering feedback action. The feedback controller assumes the responsibility of eliminating the error and dampening out the vibrations caused from plant uncertainty. Simultaneously, feedback action will also work to attenuate the disturbance signals introduced to the system during and after the slewing maneuver.

An issue that arises is the use of feedback compensation versus forward loop compensation (i.e. the use of $H(s)$ vs. $G_c(s)$ – See Figure 1-1). Whenever possible, feedback compensation should be used, since it allows the insertion of a pure zero without a corresponding pole into the transfer function. Inserting a pure zero in the transfer function means implementing pure derivative action; physically speaking, it allows the data from a rate gyro to be used for the control scheme to facilitate in vibration damping. Should an antenna-mounted angular accelerometer be available, the disturbance signal can be further anticipated and compensated accordingly to minimize vibration. Only after feedback compensation is fully taken advantage of is the design of the forward loop compensator, $G_c(s)$, considered.

The control problem being addressed is a tracking controller design problem and not a regulator design problem. Cognizant of the fact that the antenna slewing maneuver might induce vibrations, a preliminary investigation is conducted to establish a safe feedforward slewing maneuver command. The feedforward slew command is designed such that a smooth slewing maneuver ensues and at the conclusion of the slewing maneuver little residual vibrations are experienced, which requires avoiding the excitation of the first structural mode.

Furthermore, in view of the parsimonious use of feedback credo, the nominal plant information available is used to design a filter which, in the absence of plant uncertainty and disturbances, will yield the desired slewing trajectory. The filter effectively smoothes the input reference signal, θ_r, to match the output of the feedforward slew command, such that there is minimal compensation error for the feedback compensator. Hence, slewing performance is achieved using feedforward control, and

feedback control is exclusively tasked with addressing plant uncertainty and disturbance rejection. The herein envisaged control concept is illustrated in Figure 1-3.

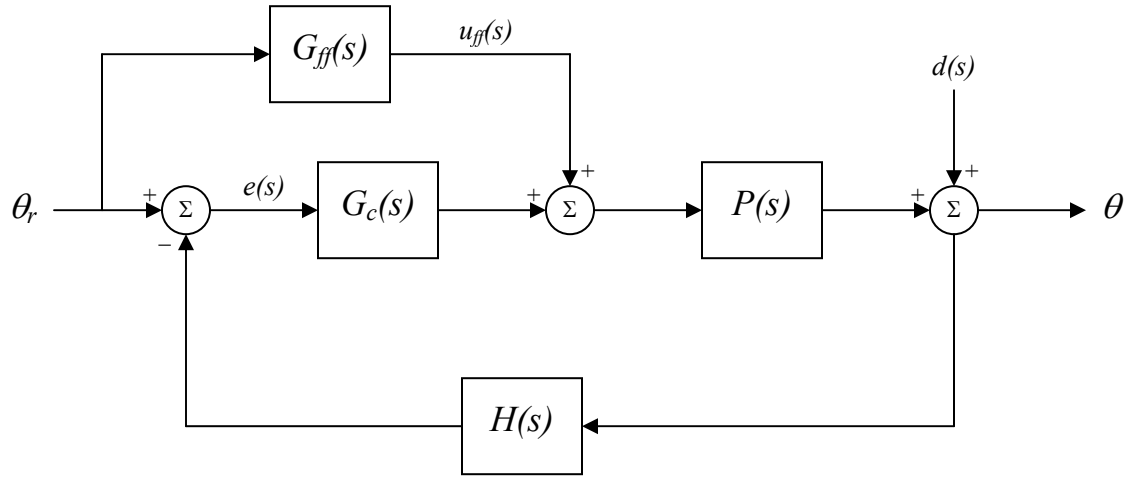

Figure 1-3: Feedforward/Feedback Control Concept

1.5. Preview

The paper is organized as follows. Literature of previous work involving feedforward and feedback control is reviewed in Chapter 2. Concepts such as optimal feedforward control and the design method of QFT are summarized. Chapter 3 outlines the design of the feedforward controller, and the determination of the slewing maneuver which reduces the excitation of modes. The design of the feedback control system is also discussed in Chapter 3. The simulations of the full control system and results are presented in Chapter 4. Also included in Chapter 4, are the comparisons to pure feedback and pure feedforward control to the combined control system. Results of the simulations involving plant variations are also presented in Chapter 4. Concluding remarks are made in Chapter 5.

II. Literature Review

2.1. Chapter Review

The purpose of this chapter is to provide appropriate background information for the concepts that have motivated this investigation. Among such concepts are Quantitative Feedback Theory (QFT), torque shaping for feedforward slewing commands, and modal suppression in feedback control.

2.2. Background of Flexible Structure Control

Some typical spacecraft operations involve slewing a structure from one attitude at rest to another attitude, bringing it back to rest. That is to say, at the conclusion of a slew maneuver, the slew rate and all of its derivatives should all be brought to zero. The open loop control problem inherent in this task is to avoid excessive structural deformation and flexible mode excitation. In the case of flexible structures, the problem becomes increasingly difficult as the magnitude of the attitude change is increased and the time to slew is decreased.

The most significant problem with attempting to control a flexible structure is the avoidance of flexible modes. In the simple case of a cantilever beam, several sensors are required along the beam to determine the shape of the modes that are excited. For large flexible space structures, several sensors would be required to determine the mode shapes and natural frequencies. More sensors are required to discern larger numbers of modes. While dealing with a large number of modes, a multi-sensor/multi-actuator strategy would likely be an excellent solution, since it can determine and shape the structure as desired. However, the ability to observe – and consequently control – the excitation of

flexible modes becomes increasingly difficult and rather expensive. Because of cost constraints, control systems typically have a single actuator to control the entire structure. The natural solution for single actuator control is to mitigate the excitation of flexible modes either through active feedback control to suppress the modes or feedforward torque shaping, which focuses on smoothing input torques to minimize the excitation of flexible body modes.

2.2.1. Open Loop Control

The equations of motion for rigid body rotation are normally described with a set of nonlinear ordinary differential equations with a frame of reference on the rigid body. Including flexible modes to the equations of motion adds an additional set of nonlinear partial differential equations. The solution of this hybrid set of equations does not have a closed form solution (Merovitch and Quinn, 1987:302). Thus, perturbation methods are normally used to find the time domain response for a given control input.

Early research has shown that shaping the torque input to the main body of the structure to the following function in Equation 2-1 will satisfy the terminal and initial boundary conditions of the response provided that there are as many degrees of freedom as constraints. The boundary conditions are that the modes and respective derivatives are zero, initially and at the conclusion of the maneuver. Therefore, the more modes which need to be controlled, the more complex the input function becomes. In Equation 2-1, *M+1* is the number of modes that need to be controlled.

$$u(t) = \sum_{n=1}^{M+1} e^{-\sigma_n t}\left(g_{1,n}\cos(\omega_n t) + g_{2,n}\sin(\omega_n t)\right) \tag{2-1}$$

Initially there are four degrees of freedom in the function *u(t)*. An additional constraint is to minimize the control effort, $u(t)^2$. The result is that the values of σ_n and ω_n have closed form solutions as a function of the equations of motion of the structure. Therefore, the number of initial and final boundary conditions constraints are the same as the number of degrees of freedom, $g_{1,n}$ and $g_{2,n}$ (Swigurt, 1978: 1-2), and the input can be derived.

Although this is the method Swigurt uses, the minimization of the control effort is not often the integrand used for optimization. Often, the main focus in optimal control is to minimize the deflection angles (and its derivatives) of the flexible appendage. The deflection angle is the difference in the angle of the appendage from the undisturbed appendage of main body. This type of optimization tends to focus on the optimal slew maneuver profile and its derivatives rather than the control input.

Research in minimizing the appendage deflection has shown that the product of the lowest structural frequency and the length of time to maneuver has a significant impact on the amount of excitation in the maneuver. Specifically, when the product is less than 5 *rad*, the excitation penalty is large when the structure is attempted to be brought back to rest at another angle. If the modal frequency is too low, the structure will be unable to keep up with the angle demanded for the rigid body; thus, at the conclusion of the slewing maneuver, the angular velocity is not zero and the structure is not brought to rest (Farrenkopf, 1979: 491-498).

There are several other methods of "optimizing" the slew command. Each research method generally chooses a quadratic cost function which minimizes control effort, flexible mode deflections, and/or flexible mode excitation (rate). Markley takes a

strategy of finding an optimal control function by minimizing the control effort, flexible mode deflection, and the flexible mode excitation. Second, Markley develops an optimal control to minimize just the flexible mode deflection and flexible mode excitation. Then he implements a third non-optimal control function which is a polynomial in time. All three solutions are compared in simulations. Similar to Farrenkopf, Markley found that the mode excitations were heavily dependent on the time interval allowed for slewing rather than the values in the weighting function. Consequently, Markley concluded that if the time interval to slew were increased by ten percent, the non-optimal polynomial control solution prevents modal excitation nearly as well as the optimal solution. He speculated that although more simple, a polynomial control function may be more sensitive to plant uncertainty and modeling errors (Markley, 1979: 625-647).

Another theory to avoid modal excitation was to ensure that the frequency content of the input signal notched the first flexible mode. Alfriend, Longman, and Bercaw disproved this theory. Using an optimal control input from Swigart, they found that the location of notches (i.e. no frequency content) in the frequency content were dependent on the length of the time of the input signal. Thus, as the time interval of the control input was varied, the notch moved away from the resonant frequency of the first structural mode, yet the control input did not induce structural excitation in the time domain. The conclusion was that there is no relationship between the frequency content of the control input and the resonant mode in optimal slewing (Alfriend et. al., 1979: 65-72).

2.2.2. Feedback Control

Meriovitch and Quinn use both pole placement techniques, as well as an optimal control strategy, to minimize the control effort and elastic energy. Bang-bang optimal control is used to slew the rigid body of structure. Pole allocation is used for feedback control to suppress the modal excitations. Here they presuppose the implementation of sensors at every node and multiple thrusters along the flexible appendage. When this sensor configuration is allowed, direct feedback control can be implemented. To minimize feedback control effort, the poles are placed such that the structural natural frequencies are the same, but the damping ratio is increased from their original values and uniform for all the considered modes. The result is that all modes decay at the same rate, and is limited only by actuator location and saturation (Merovitch and Quinn, 1987: 301-328).

Multiple sensors and actuators are not a stringent requirement on feedback control, but the control theory is simpler. Several authors have used feedback control for single input single output representations of the non-rigid plant (Junkins and others, 1990; Schoen and others, 2003). Their findings are presented next.

2.3. Modern Developments and Current Motivations

Modern developments in feedback control for the suppression of flexible mode vibrations have shifted away from optimal solutions and towards an all encompassing adaptive control theory. Several authors have claimed to developed novel techniques of identifying plants and algorithmically deriving control systems insensitive to modeling errors and external disturbances (Schoen and others, 2003: 4585-4589; Song, 1994:2872-

2876). An algorithmic strategy has its benefits, but the model is assumed to be simplified to the first flexible mode. This assumption is reasonable if the other modes are assumed to have higher frequencies and have higher damping factors.

An algorithmic approach is relevant in this current investigation, although the higher modal frequencies are not sufficiently far enough from the first flexible mode frequency to base a controller design on only the first mode.

Junkins, Rahman, and Bang take an approach to find a near-minimum time slew maneuver using the Lyapunov control law design method. The control techniques used here greatly influenced this current investigation. Feedforward and feedback tracking control laws were utilized in their design. The attempt in their investigation is to accommodate an optimal solution to other performance indices such as external disturbances and plant uncertainty (Junkins, Rahman, and Bang; 1990).

A smooth target trajectory was used rather than a step command to smooth the departure from a steady-state condition and the arrival at a new steady-state. This technique is used in this investigation to reduce the control effort of the feedback control system. Junkins admits that experiments must be conducted with a nominal model for the pre-calculation of an appropriate control solution to fit the smooth trajectory. Junkins research becomes the principle basis of the open loop experimentation conducted in Chapter 3.

2.4. Quantitative Feedback Theory (QFT)

QFT has motivated much of the methods in this investigation of determining the robustness of the controller in the face of plant uncertainty and external disturbances. All of the research in QFT for this investigation was developed by D'Azzo and Houpis.

QFT is a design method in the frequency domain of interest (i.e. the controller bandwidth, disturbance frequency content, etc.). Essentially QFT defines the boundaries of possible plants (due to uncertainties and modeling errors) and defines the limits of acceptable disturbance sensitivities and ensures that a controller is designed within the limits of the worst case scenario. QFT yields a single control solution which is valid for all configurations of the system plant. Conversely, when designing for the nominal plant, one can see how much the uncertainties can vary before stability or other system specifications are violated.

2.4.1. Parameter Variations

The open loop frequency response of the plant and compensator is first modeled on a Nichols Chart (or Bode plot). As plant parameters are varied, there is a change in magnitude and phase of the frequency response. The Nichols Chart directly correlates the closed loop response magnitude and phase. The upper and lower limits of variations are plotted in the frequency domain to obtain an area of possible plants in the frequency domain. For each parameter being varied, the maximum variations in the frequency response can be plotted on the Nichols Chart to see the corresponding closed loop system performance.

In the case for designing for the nominal plant, unique Bode plots for a frequency range of interest can be generated to see the effects on the variation of the plant. The worst case plant can be chosen based on gain and phase margins and other frequency response performance specifications. The controller should then be designed for the worst case plant such that it still meets all performance specifications in the worst case scenario.

In this investigation, the compensator is designed for the nominal plant prior to any considerations of plant uncertainty. The compensator is not designed the frequency domain for a variety of possible plants. Rather, the compensator is designed in the time domain, and the variation of plant parameters is evaluated in time domain, and the sensitivity is evaluated in the frequency domain.

2.4.2. Disturbance Rejection

Typically the specifications of the disturbance sensitivity transfer function are that it be under some magnitude over the bandwidth of the disturbance signal. Therefore there are only upper limits of disturbance sensitivity frequency response. For this investigation the specifications are that the disturbance sensitivity must be below -6 dB over a bandwidth of 0.1 to 50 Hz. The effects of plant variation on the disturbance sensitivity frequency response should be taken into consideration, as the magnitude will change with variations in plant parameters.

2.5. Key Research Points Used in This Investigation

Most of the motivation of design techniques came from Junkins, Rahman, and Bang and their development of near-minimum time slew maneuvers. One key point

taken is the determination of a priori control input which gives a smooth trajectory maneuver. The use of feedback and feedforward control by Junkins is paralleled in this investigation as well.

The QFT design method has motivated the study of plant variation of the effects of the controller. In QFT the controller is nominally designed with the foresight of the worst case plant, in this investigation QFT is used primarily as an iterative tool. That is to say, the controller is first designed to meet performance specifications; then with QFT analysis, the controller is adjusted to meet performance specifications for the worst case plant.

III. Methodology

3.1. Chapter Overview

The purpose of this chapter is to derive the design of both the feedforward controller and the feedback compensator. The feedforward controller is designed to achieve adequately quick slewing performance without inducing vibrations from the high frequency structural modes of the plant. The feedback compensator combines lead compensation with proportional gain feedback to the output signal and its derivatives. The resulting compensator damps out vibrations that may have been induced from the feedforward controlled slewing maneuver as well as attenuates the disturbance signal present in the system.

Furthermore, experiments are conducted with the entire control system to include disturbances and antenna plant variations. The methods of quantifying the effectiveness of the control scheme and justifications of comparison are discussed in this chapter.

3.2. Actual Plant Model

The actual spacecraft mounted antenna model used in this investigation is presented in a linear time-invariant transfer function provided by the sponsor in a MatLab script file. For the purposes of this investigation, the provided model is used as the nominal plant. It is assumed that the provided plant model is the creation of a SYS ID process. The truth model and its parameters are specified in Appendix A.

3.3. Feedforward Design

Two approaches to the design of the feedforward control input are investigated. The first approach entails conducting simulation experiments on the nominal plant model with known inputs to learn how the plant responds to torque inputs. The second, a model following approach, entails the synthesis of a feedforward controller $G_{ff}(s)$ using plant inversion so that a well-behaved second-order response is automatically obtained.

In regards to the first approach, the plant was first assumed to be a simple rigid body with a flexible appendage. Since the actual plant model is given in transfer function form, it is difficult – or impossible – to understand what is physically happening in the slew response. When further insight was needed, a simple model was employed since it gave a state-space physical representation of the plant. The experimentation and simulations on this model are shown in Appendix B.

It was decided for simplicity in the simulations that a direct input of a known torque command would be better simulated than the use of a feedforward transfer function controller due to numerical instabilities in implementing a feedforward transfer function. However, both techniques provided suitable responses.

3.3.1. Design by Experimentation

Open loop simulations with known torque inputs designed to perform the antenna slewing maneuver are conducted on the nominal plant model to determine what types of inputs would and would not excite the flexible modes. Two types of torque inputs were considered in the investigation of an appropriate slew response. The first is a doublet – where a positive pulse was commanded over a certain time duration followed by a

negative pulse given over the same time duration. This input was chosen because it was expected that it would excite the flexible modes of the system. The second type of input was a single sine wave. This input was chosen because it is more continuous; therefore, a more practical type of input. When integrated over time, an input signal that yields zero will result in slewing the structure from one angle to another, assuming that there are no other external forces. In other words, the total input energy should be zero for the structure to steady itself at another attitude. Both of these input signals satisfy this requirement. Figure 3-1 shows the two inputs over the same time duration of three seconds.

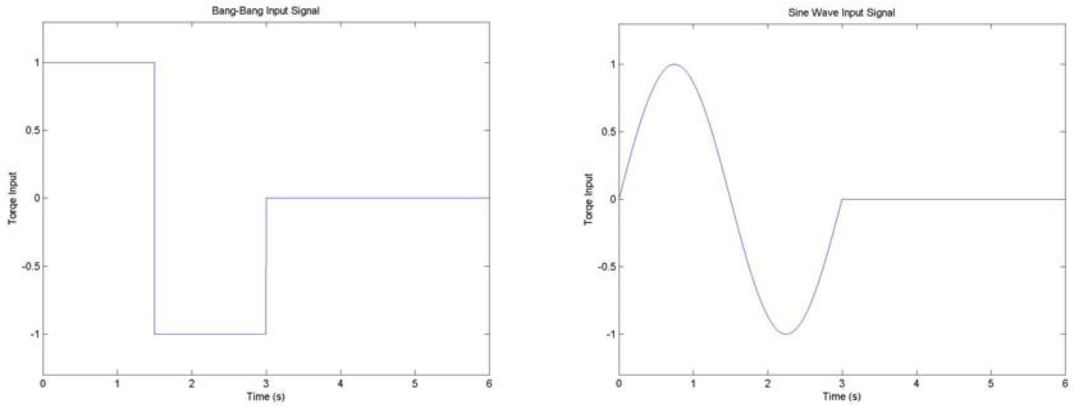

Figure 3-1: Doublet Input (Left). Single Sine Wave Input (Right)

Given that the highest structural mode of the provided plant model is about 80 Hz (see Appendix A.2), the simulation sampling frequency needs to be at least ten times that frequency; so a time step of 0.001 seconds is chosen for the simulation. This time step insures that all flexible modes are captured in the time domain simulations.

The simulations on the simple plant indicated that the input signal duration should not be close to the time period of any of the resonant structural modes – See Appendix B. With the simple plant, inputs with relatively short input durations which corresponded to

frequencies higher than the structure modes were used to avoid the time period of the resonant modes. However, this same technique could not be implemented on the actual plant due to actuator saturation limits and an unnecessarily high sampling frequency. The only other option would be to investigate time periods longer than the structural modes' frequencies.

The bare structure of the truth model (See Appendix A.2) was simulated with the doublet and single sine wave input in an attempt to learn how the structure would respond to and vibrate with these inputs. For input time durations of 2, 4, 6, 10, 16, and 20 seconds, there is little to note on the structure response as far as mode excitation. All responses demonstrated a well-behaved slewing maneuver with a smooth transition from one angle to another.

The response to the doublet input with a short two second duration is shown in Figure 3-2. As shown in the slew rate plot, vibrations are evident in the response; however, they did not seem to appreciably disturb the slew angle.

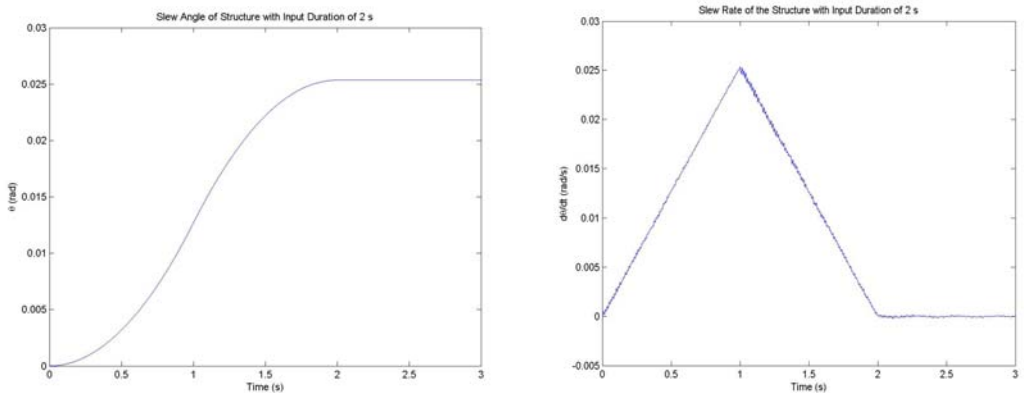

Figure 3-2: Slew Response of Antenna Structure with a Two Second Input Duration

As the input durations increased, the vibrations were less and less noticeable. Shown in Figure 3-3 are plots of the simulation results where the input duration was

increased to six seconds. With a doublet input with a duration of six seconds, the vibrations are barely recognizable on the slew rate plot. On the slew angle plot, the vibrations are unnoticeable, even on a microradian scale.

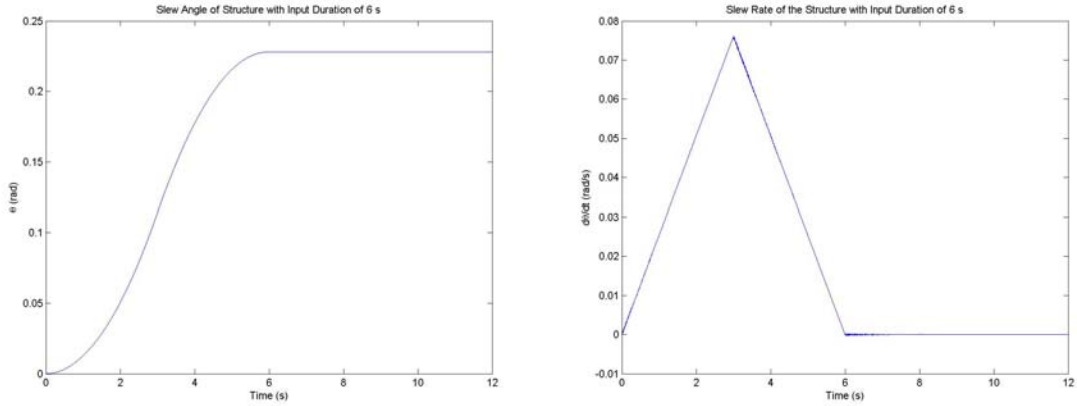

Figure 3-3: Slew Response of Antenna with a Six Second Input Duration

Since the input duration of 2 seconds did not significantly induce vibrations, inputs with shorter time durations are simulated to excite the modes of the structure.

When the doublet input duration is 0.05 seconds, excessive vibrations are induced in the structure. Shown in Figure 3-4, it can be seen that vibrations of about 21 Hz are in both the slew angle and the slew angle rate, long after the input has ended. This correlates to the first harmonic of the base cycle of the input signal (which would be 20 Hz). Evidently, the input excited the 21 Hz mode in the flexible antenna structure model. Additional simulation experiments suggest that the residual vibrations of the antenna are dominated by the closest mode to the base frequency of the input (i.e. base frequency of a 2 second input is 0.5 Hz), but residual vibrations from the other flexible modes are present in the residual vibrations as well.

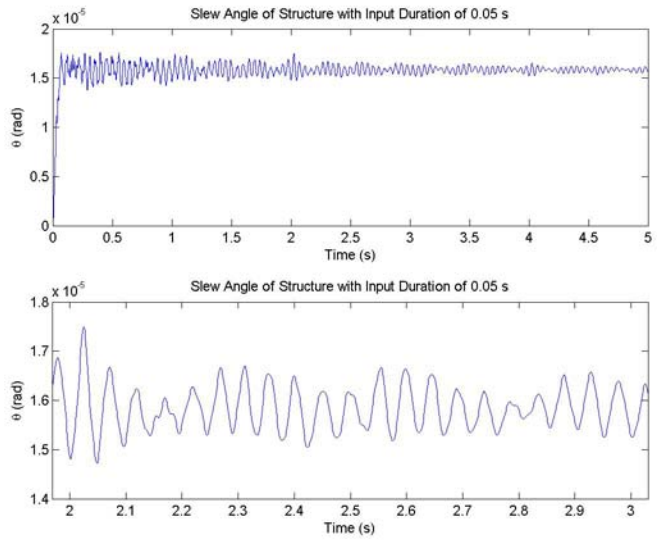

Figure 3-4: Slew Angle Simulation with a Doublet Input Duration of 0.05

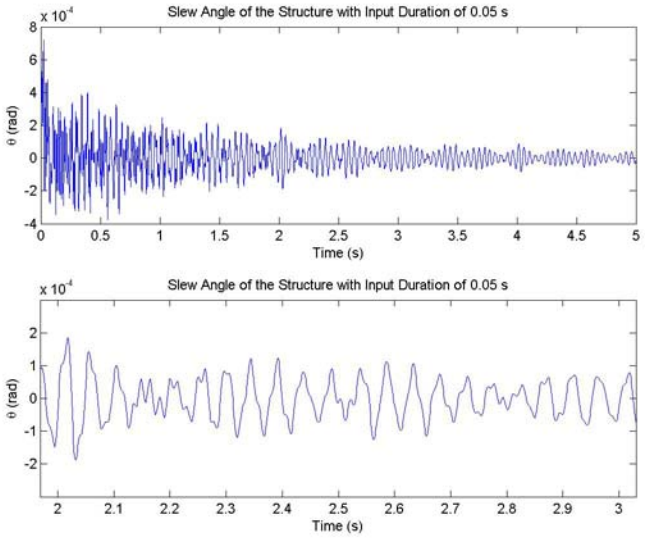

Figure 3-5: Slew Rate Simulation with a Doublet Input Duration of 0.05

The extremely low structural damping ratio is better depicted in Figure 3-4 and 3-5, as the damping is evident over time, however it does take a long time to settle. Even though the system is only vibrating $\pm 0.5 \times 10^{-5}$ radians, the amplitude of the input torque was only one oz-in. Should the input torque amplitude be increased, the vibration amplitudes would increase linearly.

From the previous simulations, it can be deduced that the lower the time duration of the input (doublet or single sine wave), the more vibrations are induced. Therefore, slewing maneuvers with longer time durations are preferable over those with short ones. Longer slewing maneuvers avoid the high frequency flexible modes of the antenna structure. Longer slewing maneuvers yield higher slew angles and induce little to no vibration and reach a steady-state in a reasonable amount of time.

Although the structure simulations show that the feedforward torque inputs should have longer durations, the other components of the antenna plant have not been included in this portion of the investigation. The angle rate sensor (ARS), anti-aliasing filter (AAF), and the A/D converters do not significantly contribute to the dynamics of the response. The frequency responses of those components show perfect tracking with unity DC gain and a bandwidth of about 30 Hz. However, the motor dynamics do not have the same benign tracking characteristics as the ARS, AAF and the A/D converter. Hence, the simulation experiments with the doublet and single sine wave inputs are repeated to include the motor and structure combined.

The motor Bode plots are shown in Figure 3-6. There are two types of motors: a high gain, and a low gain motor. As seen in the Bode plots, the high gain motor amplifies the input signal by roughly three orders of magnitude and the low-gain motor decreases the signal by about one order of magnitude.

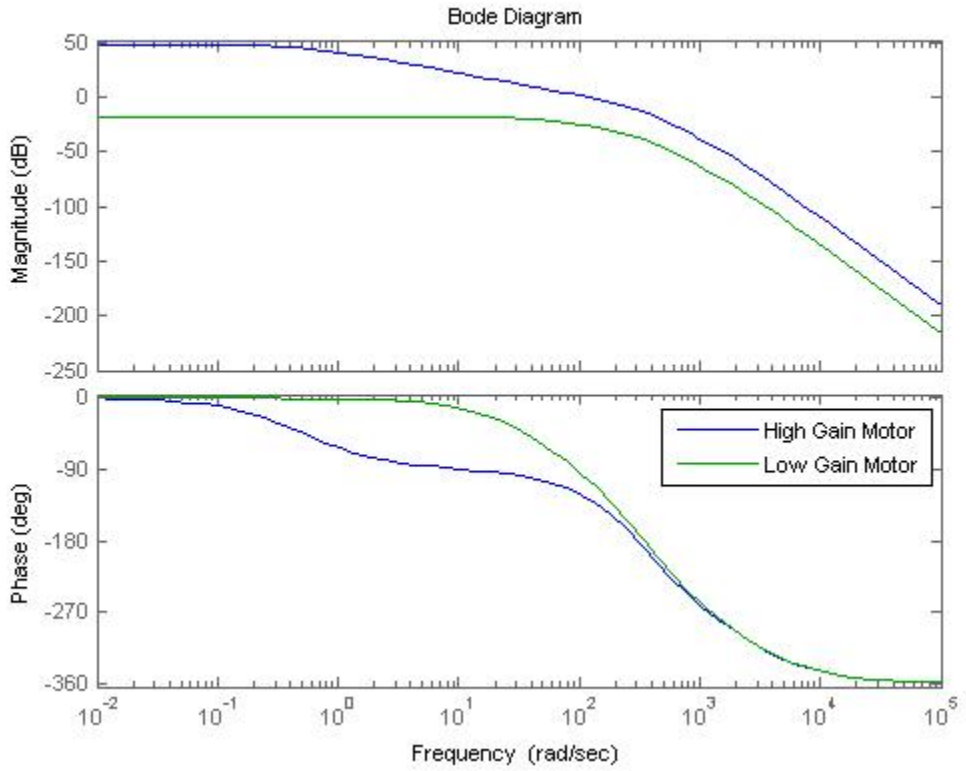

Figure 3-6: Frequency Response of the High Gain motor (Blue) and Low Gain Motor (Red)

Figures 3-7 and 3-8 show the responses to a doublet input on the combined high-gain motor and structure. The input duration here is 0.05 seconds again. The high-gain motor does not seem to induce vibrations to the system that are evident in the simulations without the motor. However, similar to the plot of the two second input signal applied to the bare structure (see Figure 3-2), the vibrations are evident in the plot of the slew rate. Key points here are that the settling time of the high gain motor-structure combined is much longer than just the structure, but the final slew angle is much greater.

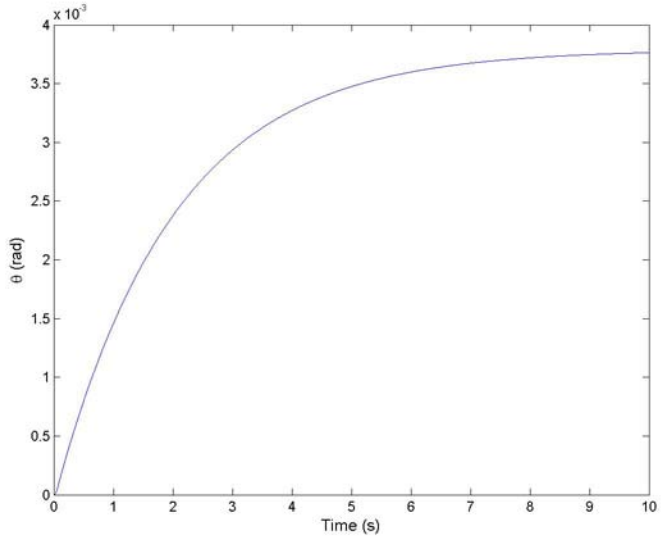

Figure 3-7: High Gain Motor-Structure Slew Angle Response with a Doublet Input Duration of 0.05

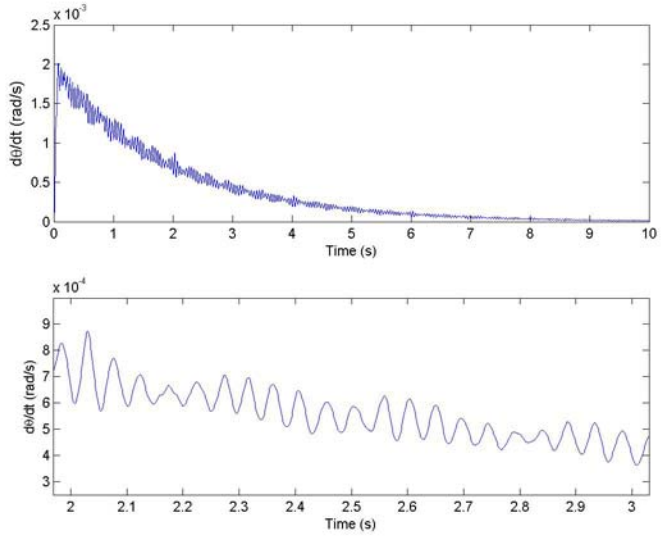

Figure 3-8: High Gain Motor-Structure Slew Rate Response with a Doublet Input Duration of 0.05

The low gain motor/structure combination displayed similar responses to the bare structure. As suggested by the Bode plots, the final slew angle is about one-tenth of that of the simulation of just the structure. The low gain motor and structure respond much faster and reach a final slew angle much faster than the high gain motor/structure does. However, the vibrations are excessive. This is attributed to the respective bandwidths of

the two motors. The low gain motor has a significantly higher bandwidth. The low gain motor's bandwidth is 8 Hz while the high gain motor's bandwidth is 0.05 Hz.

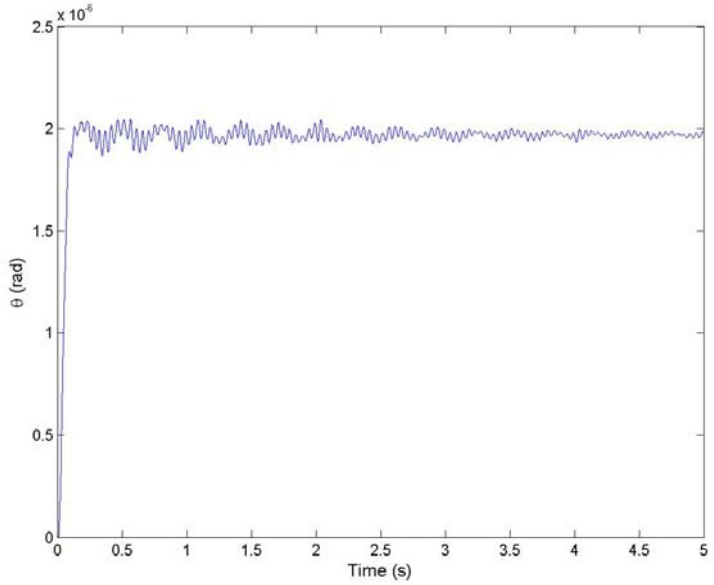

Figure 3-9: Low Gain Motor-Structure Slew Angle Response with a Doublet Input Duration of 0.05

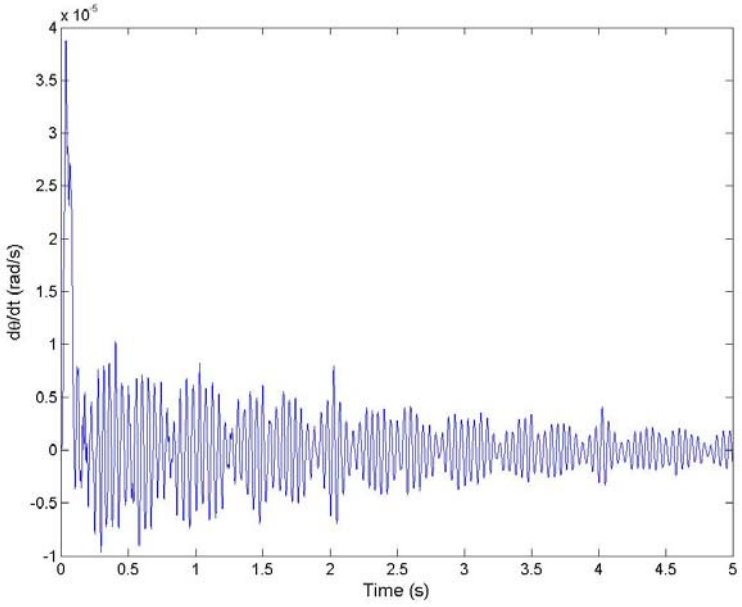

Figure 3-10: Low Gain Motor-Structure Slew Rate Response with a Doublet Input Duration of 0.05

The previous simulations suggest that the low gain motor is best used to slew the antenna. However, the response is relatively small (microradian slew maneuver) due to the fact that the torque amplitude only reached 1 *oz·in* and it was only implemented for a duration of 0.05 seconds. It does beg the question as to which gains would be best used for control. Since the accuracy specifications require that the response remain within five microradians of the desired response, small and fast inputs from the low gain amplifier motor result in residual vibrations that are within those performance specifications.

With a low gain motor, the response to inputs is faster than the response from the high gain motor. However, since the high gain motor gave a smoother response (see Figure 3-7), it may be used best for damping out the vibrations induced during the period where the low-gain motor is used. The low gain motor should be used to slew the structure over some time period with an open-loop input to the plant; then, the high gain motor should take over with feedback control and dampen out the induced vibrations. The complexity of such dual mode simulations where one switches between the motors is avoided by eliminating the amplifier gains from further investigation. The low gain motor transfer function structure is used and is multiplied by a gain such that the open loop frequency response at low frequencies has a magnitude of 0 dB, or a DC gain of 1 (See Appendix A.3). This then correlates to a steady-state output torque of 1 *oz·in* when the commanded torque is 1 *oz·in*.

3.3.2. Implemented Feedforward Signal

The feedforward signal is a single sine wave with a frequency of $2\pi/\tau_d$, where τ_d is the desired time duration of the feedforward input signal. The final slew angle from the

feedforward signal is dependent on the amplitude of the torque and the duration of the input signal. Without loss of generality, the desired final slew angle is chosen to be one radian.

Considering only the rigid body mode, the equations of motion of the antenna are

$$\ddot{\theta} = bu, \quad \theta(0) = \dot{\theta}(0) = 0, \quad 0 \le t \le \tau_d \,, \tag{3-1}$$

where u is the feedforward input signal and b is the inverse of the antenna rigid body moment of inertia – see Appendix A.2. The input signal is

$$u(t) = \begin{cases} 0, & t < 0 \\ A\sin\left(\dfrac{2\pi}{\tau_d} t\right), & 0 \le t \le \tau_d \\ 0, & t > \tau_d \end{cases} \tag{3-2}$$

where, recall, τ_d is the desired time to slew, and A is the amplitude of the torque in *oz·in*. Solving Equation 3-1 yields:

$$\theta(t) = \frac{-bA\sin\left(\dfrac{2\pi}{\tau_d} t\right)}{\left(\dfrac{2\pi}{\tau_d}\right)^2} + \frac{bAt}{\dfrac{2\pi}{\tau_d}} \tag{3-3}$$

at the time to reach a final slew angle, $t = \tau_d$, the slew angle is

$$\theta(t_d) = \frac{-bA\sin(2\pi)}{\left(\dfrac{2\pi}{\tau_d}\right)^2} + \frac{bA{\tau_d}^2}{2\pi} = \frac{A{\tau_d}^2}{J_{inertia}\,2\pi} = 1 \text{ rad} \tag{3-4}$$

3.3.3. Design by Plant Inversion

It is assumed that the plant model is determined from system identification. Although the plant model is not completely accurate, the obtained plant model is used as

the nominal plant to be controlled. Thus the open-loop feedforward controller transfer function can be derived from the nominal plant, the modeling errors being ignored and considered to be handled by the feedback controller.

To determine the desired feedforward transfer function G_{ff}, first calculate the input signal required to give the desired response based on the knowledge of the nominal plant. Assuming that there is no feedback controller generated input, the nominal feedforward input transfer function is,

$$u_{ff}(s) = \frac{\theta_d(s)}{P(s)} \tag{3-5}$$

The actual pointing angle response is assumed to be exactly the same as the desired response. This is consistent with the idea that the feedforward controller assumes full authority for the pointing maneuver. Therefore, θ, the output of the plant, matches the desired pointing angle response of the system, θ_d. The desired response of the system is chosen to be the step response of a second order system. The transfer function of this type of system is shown in Equation 3-6.

$$\frac{\theta_d(s)}{u(s)} = \frac{\omega_n^2}{s^2 + 2\zeta\omega_n + \omega_n^2} \tag{3-6}$$

and therefore,

$$\theta_d(s) = \frac{1}{s}\frac{\omega_n^2}{s^2 + 2\zeta\omega_n s + \omega_n^2} \tag{3-7}$$

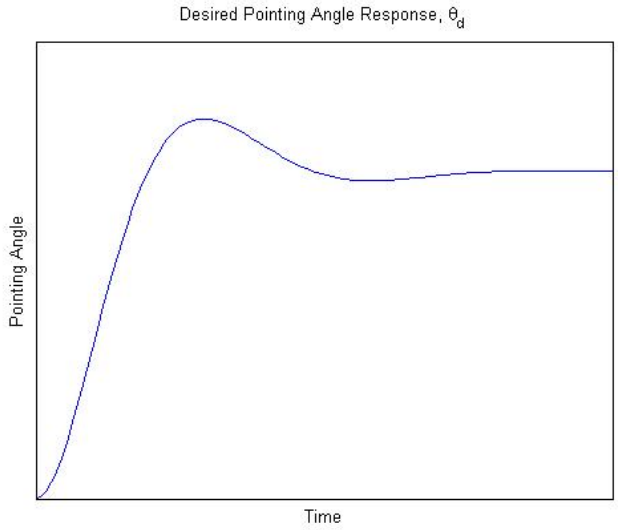

Figure 3-11: Time History of Desired Response

Combining Equations 3-5 and 3-7 and solving for the feedforward control input yields the following:

$$u_{ff}(s) = \frac{\omega_n^2}{s\left(s^2 + 2\zeta\omega_n + \omega_n^2\right)P(s)} \tag{3-8}$$

This algorithm for calculating the feedforward control input works, provided that the plant model has an excess of no more than three poles than zeros. If this is not the case, the control signal becomes improper in the frequency domain. The desired ideal response, $\theta_d(t)$, would need to be changed so that its Laplace transform has three or four poles to compensate for an excess of four or five poles over zeros.

The mechanization of the feedforward concept adds an additional transfer function $G_{ff}(s)$ which takes the reference input, $\theta_r = \theta_d$, and automatically outputs the feedforward command signal derived above. Therefore, as opposed to sending a direct feedforward signal, u_{ff}, a transfer function takes the desired slew response (i.e. the reference signal) and outputs the proper u_{ff} to slew the plant. The reference signal is

chosen to be exactly the same as the desired response, namely the output of the feedforward open loop control system. Figure 3-12 shows the block diagram of the feedforward/feedback control system mechanization.

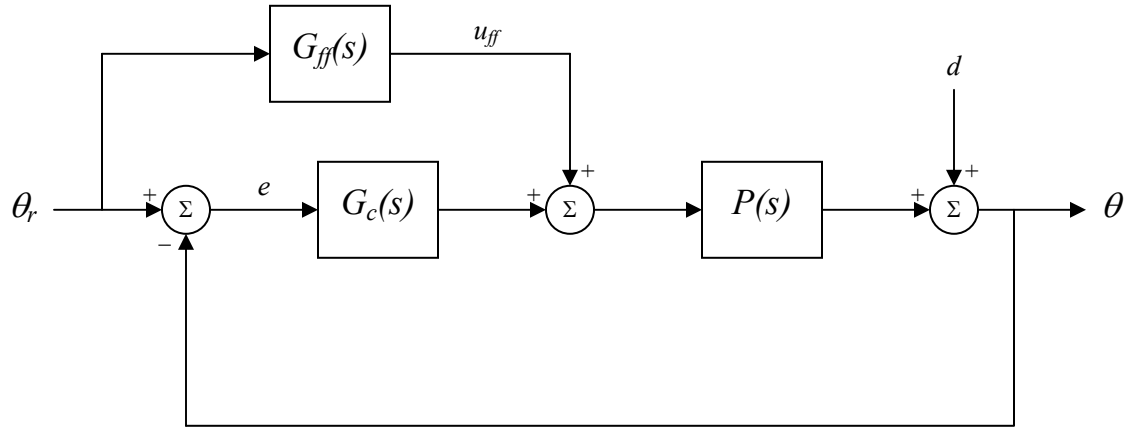

Figure 3-12: Mechanized Control System Block Diagram

The feedforward transfer function $G_{ff}(s)$ is designed by dividing the control signal $u_{ff}(s)$ by the reference input θ_d. Since the reference input is the same as the desired response of the system, the feedforward transfer function is

$$G_{ff}(s) = \frac{u_{ff}(s)}{\theta_r(s)} = \frac{u_{ff}(s)}{\theta_d(s)} = \frac{1}{P(s)} \tag{3-9}$$

This transfer function represents a pure inversion of the nominal plant model. Separating the feedforward transfer function from the feedback system, leaving only the plant and feedforward transfer function, results in a cancellation of the plant transfer function, $P(s)$. In other words, the response from the feedforward controller is exactly the same as the reference signal input because the resulting overall transfer function is 1. Thus, the desired performance is achieved without the use of feedback control in the hypothetical absence of plant uncertainty and disturbances.

In the real world the implementation of this scheme does not exactly reproduce the reference signal. Because resonances of the flexible modes are so close together in the frequency domain, inverting the modes may exacerbate the situation unless all the modes and their peaks are perfectly known. Inverting the resonant modes simply means creating a notch where there is a spike in the frequency domain, thus – with the concept of additivity – effectively cancelling out the spike.

For example, in the antenna plant under investigation, the 21 Hz mode needs to be inverted, or notched. However, if the actual plant mode was slightly off, the notch created to cancel out the 21 Hz mode, actually results in a much larger resonant spike when summed with the structure's frequency response. The system identification problem now limits the implementation of plant inversion since it may result in residual vibrations that are much worse than the vibrations excited during the open loop operation.

Typically, the imprecisely known modal frequencies will induce unexpected vibrations when the antenna is slewed. That is to say, inaccurate frequencies/modeling errors will result in a response different from the desired response. This of course reduces the robustness of this type of control; however, this problem is solved with the introduction of feedback control, which restores the robustness required for precise control of an uncertain plant.

To minimize the possibility of exciting all of the modes of the system, the feedforward controller is simplified to only invert the motor, rigid body, and the first flexible mode of the plant. As seen in most plants with flexible modes, the first flexible mode is typically the worst mode to excite because it has the greatest peak amplitude.

Further avoidance of perturbing the modes may be possible using the results found in open-loop experimentation. These inputs may be more desirable because hypothetically they do not induce any vibrations in the system response, and robustness may not be an issue as long as the modes stay within reasonable bounds. However, smooth feedforward inputs that avoid the flexible mode's excitation may prolong the slewing time required for the antenna – so there is a tradeoff.

Both the plant inversion and the single sine wave input are used to implement feedforward action. The direct injection of the feedforward input signal into the antenna plant avoids any numerical instability which may arise through the use of the feedforward transfer function, $G_{ff}(s)$. Numerical errors may arise from the pole-zero cancellations between the feedforward transfer function and the antenna plant and small errors in the poles and zeros can computationally lead to unexpected responses. Therefore to simplify the simulations, a single sine wave feedforward signal is fed directly into the antenna plant rather than implementing the transfer function $G_{ff}(s)$ to automatically create a feedforward signal based on the desired response/reference signal.

3.4. Computation of the Feedforward Signal

For the antenna rigid body, the moment of inertia J is 39.46 $oz \cdot in \cdot s^2$. Therefore, the amplitude, A, and desired slew time, τ_d, must satisfy the following requirement.

$$A\tau_d^{\,2} = 247.9345\ oz \cdot in \cdot s^2 \tag{3-10}$$

The feedforward control input is designed such that it satisfies the constraint in Equation 3-10. To minimize the time to reach the final slew angle, this constraint is normally governed by the desire to avoid saturating motor output – thus limiting the

amplitude of the torque. However, the saturation limits of the motor are unknown. In lieu of this unknown saturation limit, the time is constrained. A jittery response from the feedforward torque is still undesirable. From the bare structure simulations shown in open-loop experimentation, shorter time durations cause more residual vibrations. Therefore, an additional constraint is placed on τ_d. The time response for an input duration of six seconds shows no residual vibrations in the angle response – see Figure 3-3.

Based on the open loop simulations and justification of the utility of direct feedforward torque, the following feedforward input signal is then chosen:

$$u(t) = \begin{cases} 0, & t < 0 \\ 6.8871\sin\left(1.0472t\right), & 0 \le t \le 6 \\ 0, & t > 6 \end{cases} \tag{3-11}$$

This input signal yields the following slewing response from the entire combined nominal plant model.

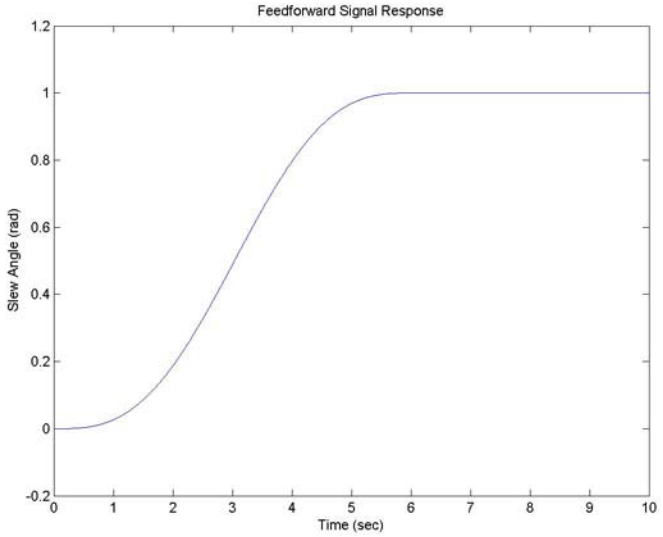

Figure 3-13: Response to Feedforward Torque

The angle response here is exactly as desired. The structure slews one radian in six seconds and little residual vibrations are induced in the structure. The final errors after a 6 second maneuver are on the order of 10^{-8} radians; therefore, the results should not be appreciably affected by the small difference between the steady-state slew angle and 1 radian.

3.5. Design of Feedback Compensation

The second step of the herein pursued control concept is the synthesis of a feedback controller. Since the model is assumed to be linear, the superposition principle allows the feedforward and the feedback controllers to be designed separately.

3.5.1. Feedback Control Theory

The feedback compensator is designed for robustness. It must reject an uncertain disturbance signal $d_2(s)$, and it must compensate for the uncertainty in the plant model. The accomplishment of these tasks is somewhat subjective. The steady-state accuracy with the disturbance signal present must be within 5 microradians. The resulting Bode plot of the compensated closed loop feedback control system should have good gain and phase margins (i.e. 6 dB and 25° respectively).

The closed loop control system is expressed as

$$T(s) = \frac{G_c(s)}{1 + G_c(s)P(s)H(s)} P(s) \tag{3-12}$$

where $P(s)$ is the plant transfer function, $G_c(s)$ is the forward path compensator and $H(s)$ is the feedback path compensator.

The sensitivity function to the output disturbance d_2 is

$$S(s) = \frac{y(s)}{d(s)} = \frac{1}{1 + G_c(s)P(s)H(s)} \tag{3-13}$$

$G_c(s)$ must be chosen so that the compensated system sufficiently rejects the disturbance signal d_2 and suppresses the effects of plant uncertainty sourced from system identification.

Feedback compensation provides derivative action by virtue of the availability of an antenna mounted rate gyro. Thus, the feedback compensation technique is implemented in both the forward path of the loop and feedback path of the loop as shown in Figure 3-14.

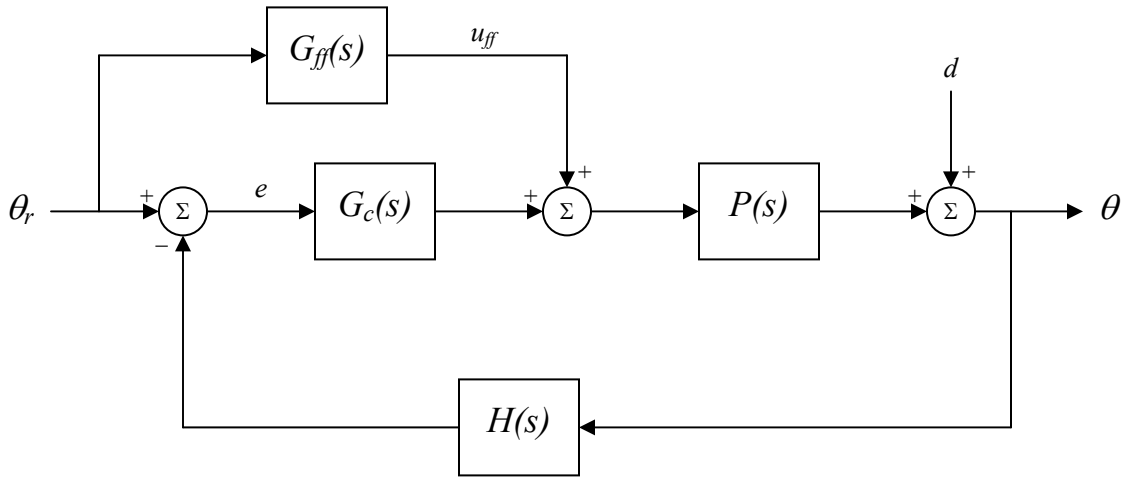

Figure 3-14: Feedback Compensation Block Diagram

Here, H is a polynomial in s of increasing derivatives of the response, θ. A hypothetical transfer function for H is

$$H(s) = k_1 + k_2 s + k_3 s^2 \tag{3-14}$$

However, Figure 3-14 is misleading in that it represents $H(s)$ as a feedback transfer function. In actuality, the diagram only signifies that derivative data is available for feedback – that is to say, the slewing angle is not the only data that is fed back to the

compensator. Rate gyros and accelerometers can measure the angular rates and accelerations of the antenna, and the data taken from these sensors allows the use of rate and/or acceleration feedback control. This type of configuration allows feedback gains to be assigned for the derivatives of the response, θ. The physical mechanization involves measuring the output angle's rate and acceleration using either an angular acceleration sensor or a pair of separately mounted accelerometers. If the use of these sensors is not available, the control problem becomes increasingly difficult.

The first term of the compensator, *H(s)*, is the angle position gain. The second term is the angular rate gain. The third term is an angular acceleration gain. If accelerometers are not available to provide the antenna's angular acceleration data, the compensator is limited to the first two terms. Otherwise, if the accelerometer data is available, then the compensator may have all three terms and the respective gains are k_1, k_2, and k_3.

Again, the objective is to lower the resonant peaks of the plant and increase the gain and phase margins of the system. To simplify the problem, the plant is reduced from having twenty modes, to having a single resonant mode. This assumption is reasonable because for typical flexible systems, after each subsequent flexible mode, the transfer function magnitude drops at an additional rate of 40 dB per decade. Therefore, provided that the frequencies of the modes are separated enough, the suppression of the first mode should sufficiently reduce the vibration level.

3.5.2. Example

An academic example of resonance suppression is presented first. It is important to note that this example assumes the availability of acceleration feedback that, unfortunately, is not currently available in the antenna control system. It is used strictly to demonstrate suitable control of a plant with a single, very lightly damped elastic mode using feedback compensation. It is also important to note that in reality there is no actual *H(s)* compensator and no derivatives are computed; instead, the derivatives are physically measured and fed back through inner loops.

The example plant has the following transfer function:

$$P(s) = \frac{16}{s(s+1)(s^2 + 2 \cdot 0.0005 \cdot 4s + 16)} \tag{3-15}$$

The plant has a single lightly damped ($\zeta = 0.0005$) mode at a frequency of 4 rad/s. It also demonstrates typical rigid body dynamics.

Feedback control is used to stabilize the highly resonant elastic mode of the plant. The feedback transfer function is chosen to be in polynomial form, as discussed previously,

$$H(s) = ks(s+1)(s+a) \tag{3-16}$$

and the compensator, $G_c(s)$, is chosen to be a constant gain K. From Equation 3-12, the closed loop transfer function is

$$T(s) = \frac{KP(s)}{1 + KP(s)H(s)} = \frac{16K}{s^2 + (0.8 + 16Kk)s + 16(1 + Kka)} \tag{3-17}$$

The resulting closed loop transfer function is a second-order system. Now the natural frequency and damping ratio can be arbitrarily chosen. To keep the physics

unchanged, ω_n is chosen to be 4 rad/s; however, the damping ratio, ζ, is increased to 0.707. The resulting values for the gains K, k, and a, can then be analytically determined in this academic example to give the desired performance results. The resulting gains are listed below.

K = 1.563

k = 0.28

a = 1.29

The resulting frequency and time responses are shown below. The designed feedback compensation has eliminated the sharp resonant spike of the original open loop plant frequency response. The time response will be much smoother with smaller and negligible oscillations.

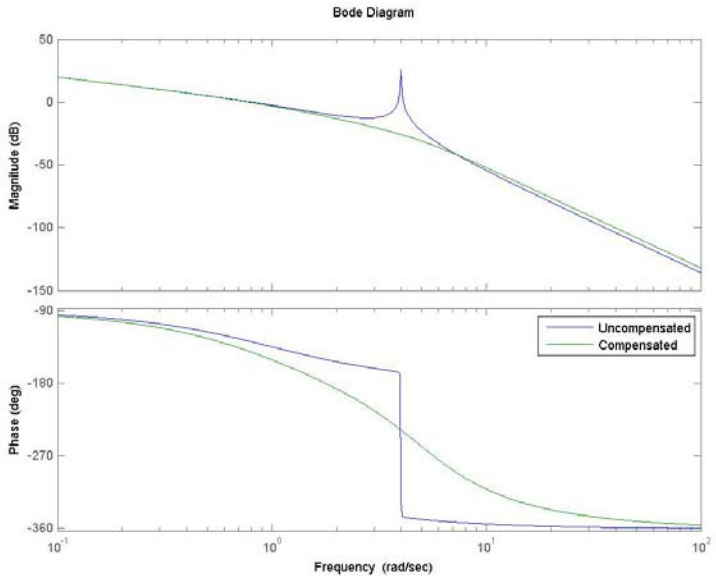

Figure 3-15: Frequency Response of Compensated and Uncompensated Systems

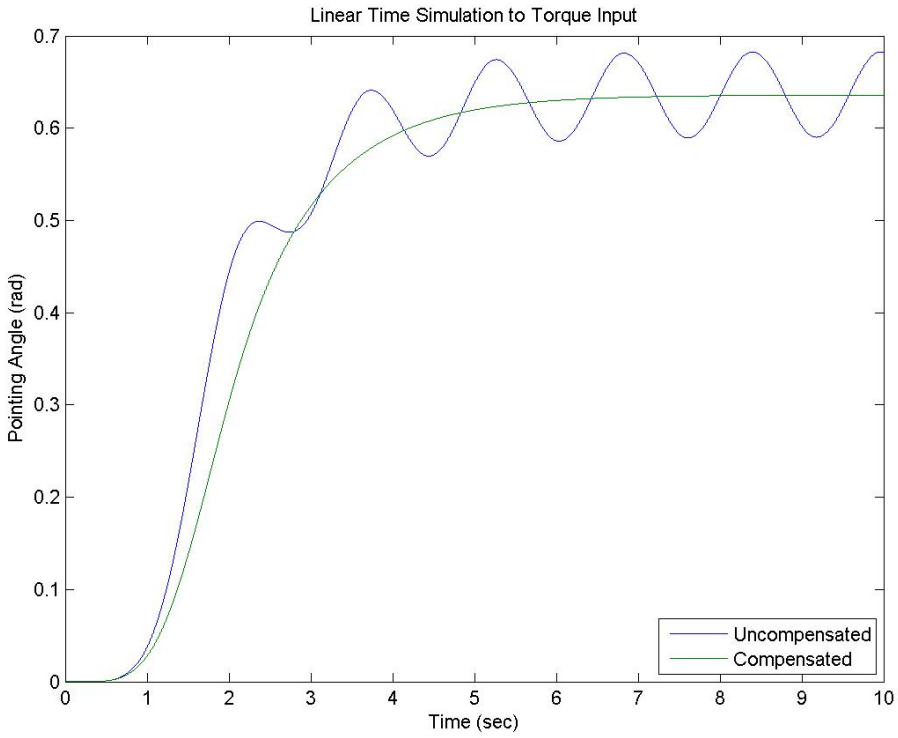

Figure 3-16: Time Response of Compensated and Uncompensated System

It is important to note that while the compensated system's frequency response presents a solution to the resonant spike, the compensated transfer function magnitude at higher frequencies is slightly higher than the uncompensated transfer function magnitude – as consistent with Bode's fundamental "waterbed" theorem. Figure 3-16 shows the time response to a single sine wave torque input of 2 seconds. The compensated systems time domain response is smooth and without noticeable oscillations/ringing.

The previous example presented utilizes higher-order sensors for the compensation. The actual mechanization of feedback control would nominally have angular acceleration and angular rate data; however, even the acceleration data may not be available. Lacking the acceleration data limits the feedback compensator, *H(s)* to, at most, a second-order polynomial.

If angular acceleration data is not available, zeros may be included in the compensator, $G_c(s)$, with an equal number of poles. Some flexibility in the design of the control system is then lost, since dynamics, in addition to the chosen dominant closed loop poles, affect the closed loop response.

3.5.3. Actual Implementation of Feedback Control

Motivated by the academic example discussed above, feedback compensation is implemented on the nominal plant as follows. The Figure 3-17 demonstrates the actual feedback control scheme. The plant transfer function, $P(s)$, takes an input torque and outputs an angular rate. Indeed, angular rate data is available for feedback control. The inner feedback loop operates on the angular rate measurement. The inner loop utilizes proportional gain feedback control, with the gain K_r, to maintain a desired angular rate. An integrator is in place so that the slewing angle data is also available for feedback. The slewing angle is fed back into a lead compensator, $G_c(s)$, which further tightens the control loop. The disturbance signal d_2 is introduced into the system to model an external angular disturbance from the host spacecraft/bus.

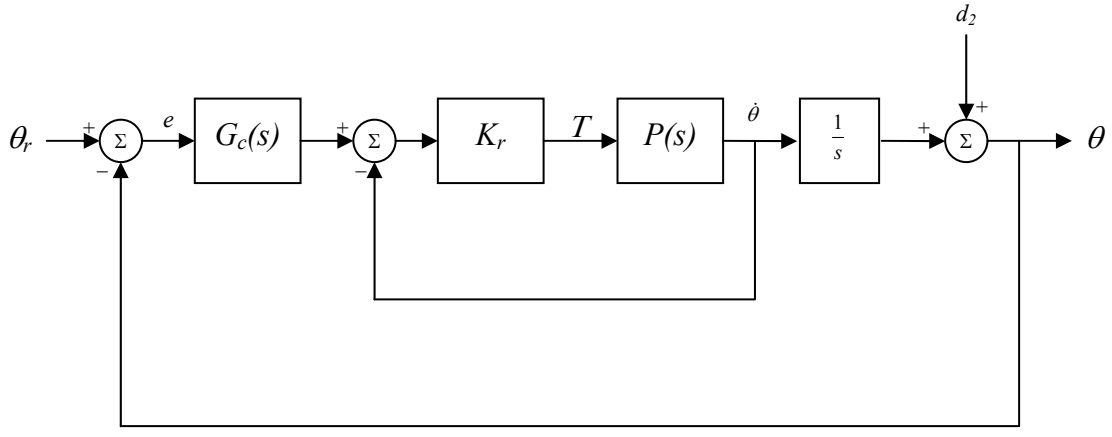

Figure 3-17: Implementation of Feedback Control

Since the feedback controller is absolved from the responsibility of slewing the structure, its design is focused on disturbance signal rejection and vibration damping and suppression.

The value of K_r and the transfer function $G_c(s)$ are determined based on root locus considerations and time domain simulations. Again, high pointing accuracy (small error) and disturbance rejection are the major factors in designing a suitable compensator. The next section shows the steps taken in choosing the feedback parameters which yield appropriate disturbance rejection.

3.5.4. Feedback Compensator Design

Since the feedforward torque input signal does not excite residual vibrations (see Figure 3-13), the main goal of the compensator is the attenuation of the disturbance signal. From Figure 3-17, the gain K_r takes an input error of *rad/s* and outputs a torque with units *oz-in*. The units of K_r are $oz \cdot in \cdot s$. The compensator G_c takes an angle error in radians and outputs an angular rate in radians per second to be differenced with the inner feedback loop. The dimension of G_c is then s^{-1}.

To begin to find values for K_r and K_p which satisfy performance specifications, the plant model is simplified and a root locus design technique is employed to see how the system poles will behave with different values of gain. For simplicity, the structure is assumed to be the rigid body with the first flexible mode; the time delays, the motor, the sensors, and the other flexible modes are ignored at this point. First, the inner loop of the control system is designed, that is, the angular rate response to a desired angular rate response transfer function. The transfer function of the simplified plant is shown below.

$$P(s) = \frac{0.025(s^2 + 0.85s + 442)}{s(s^2 + 0.83s + 430)} \tag{3-18}$$

It is seen here that the second-order poles and zeros are very close to each other and that a change in gain would not affect the location of the flexible mode poles – see the root locus plot in Figure 3-18. This is satisfactory, because the objective is not to alter the structure's flexible mode frequency, that is, to change the physics, but to satisfactorily track the commanded angular rate.

Increasing the gain, K_r, does not change the open loop second-order poles very much; it does move the free integrator pole away from the imaginary axis. By moving the pole away from the imaginary axis two things are implied. First, the farther the pole is moved away, the more the response becomes dominated by the very low damped structural modes which remain close to the imaginary axis. Second, the farther the pole is moved away, the faster the first-order response to system inputs. So the trade-off is a fast, but oscillatory response, or a slower, smoother response.

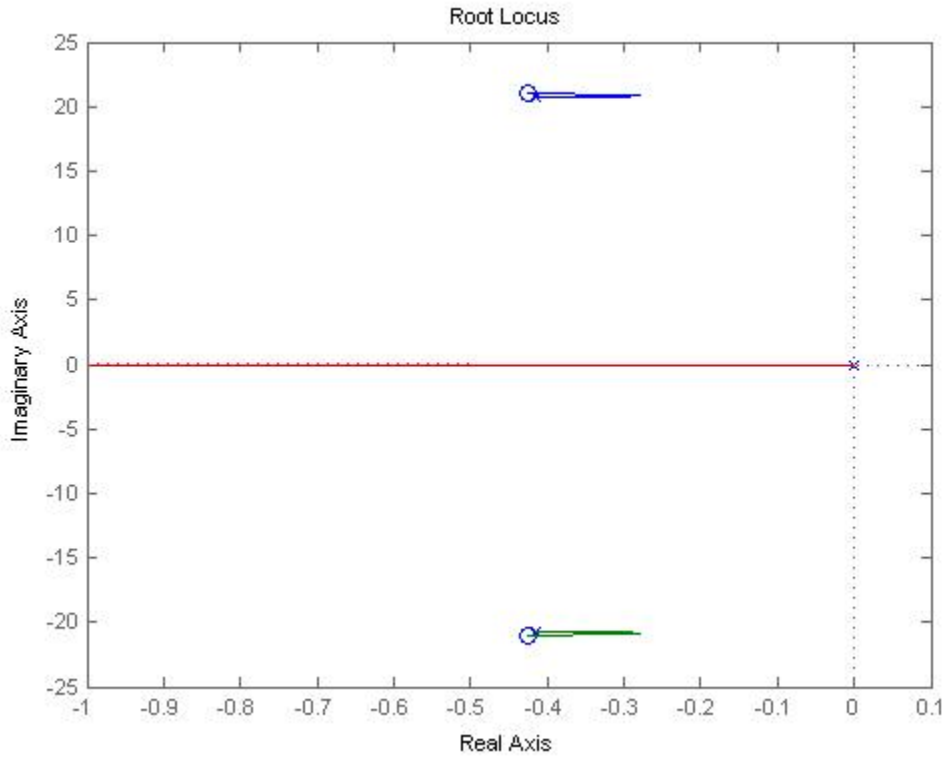

Figure 3-18: Root Locus of Inner Loop

Since the structural mode poles have a real value of about -0.4, it traditionally is not wise to choose the gain such that the free integrator pole moves farther left than that. As the pole moves farther away from the axis, the tracking error increases and the response may become dominated by the second-order poles.

Consequently, since the structural mode (i.e. second-order pole) is lightly damped, increasing the gain may make tracking very difficult. However, since there are zeros present in the system, it also may be safe to assume (as long as the gain remains reasonably low) that the zeros and the poles are close enough to each other to cancel themselves out, thus leaving a dominant first-order response.

If the gain is increased such that the pole is moved left of the second order poles, there are two possibilities. The first is that the second order poles dominate (i.e. no pole-zero cancellation). The second is that the poles and zeros cancel and first order pole remains dominant. Due to the simplicity of this model, and the difficulty of determining the final response, no definite value of K_r is chosen at this point. The simplified plant model is used and the analysis continues to the outer loop.

Once $\dot{\theta}$ is fed back using K_r, the closed loop transfer function for the inner loop is

$$G(s) = \frac{0.01(s^2 + 0.85s + 442)}{s^3 + (0.83 + 0.025K_r)s^2 + (430 + 0.0213K_r)s + 11.05K_r} \tag{3-19}$$

The next step is to determine $G_c(s)$. First, it is assumed that $G_c(s)$ is a constant gain. Therefore, the root locus method is employed again for analysis. The new open loop transfer function multiplies the closed inner loop transfer function with a free integrator (see Figure 3-17). Several root locus plots are shown below with different values of K_r. The root locus plot, with a value of K_r of 4 *oz·in·s*, is shown below in Figure 3-19. A root locus plot with a higher K_r of 40 *oz·in·s* is shown in Figure 3-20. And a root locus plot with a K_r of 400 *oz·in·s* is shown in Figure 3-21.

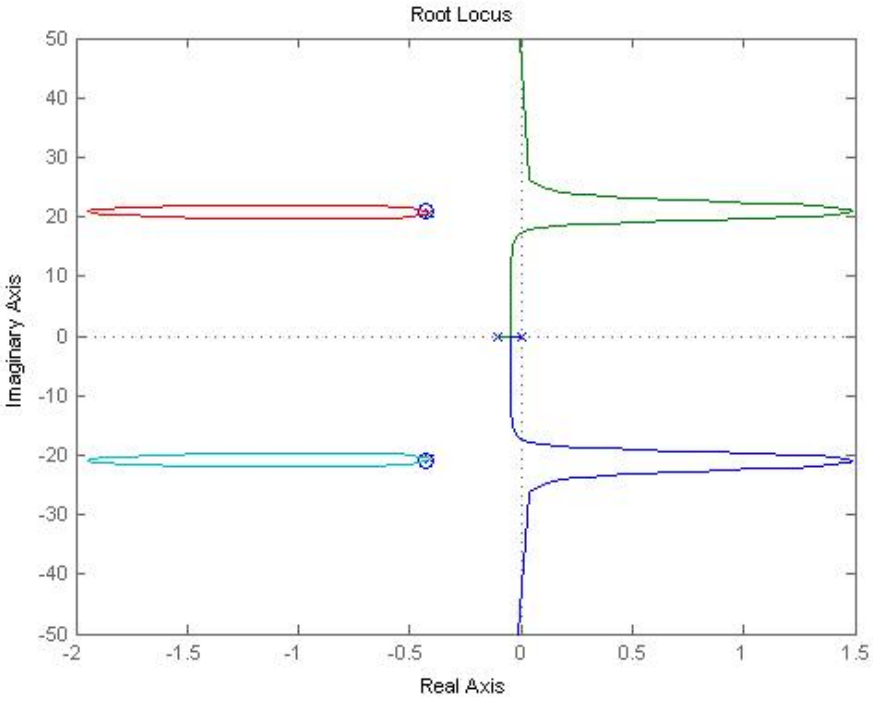

Figure 3-19: Outer Loop Root Locus with an Inner Loop Gain of 4

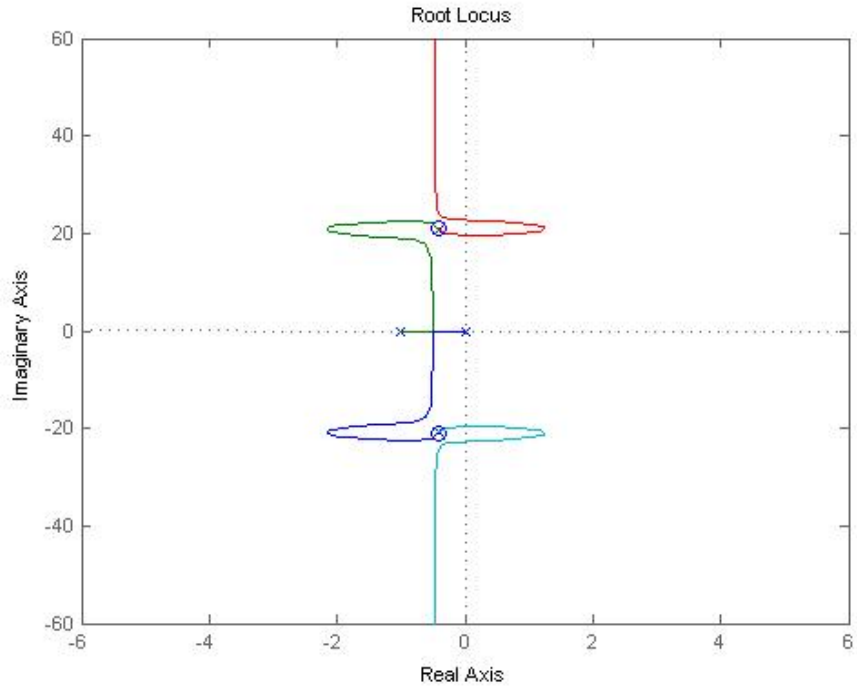

Figure 3-20: Outer Loop Root Locus with an Inner Loop Gain of 40

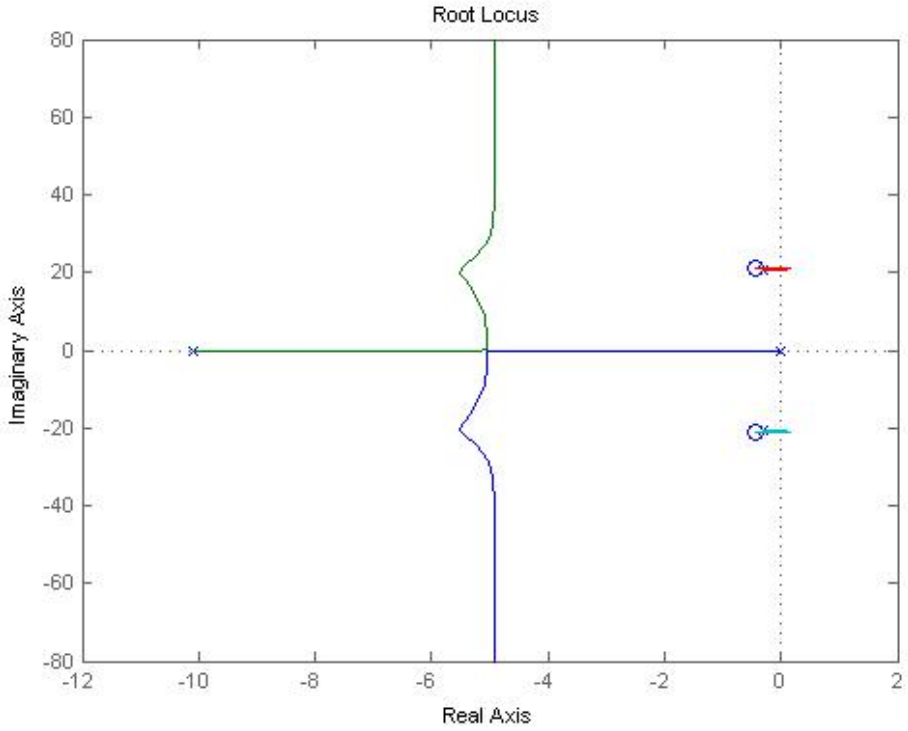

Figure 3-21: Outer Loop Root Locus with an Inner Loop Gain of 400

As the gain K_r is increased, the structural mode poles and zeros loci move toward the right half plane as the rigid body poles and zeros move further left. Instability here is not a major concern because the gains required to destabilize the system are on the order of 10^5. Since the objective here is to keep the gains as low as possible, gains of that magnitude are not taken into consideration.

Although the root locus plots do not give definite values for appropriate gains, they do give a good starting point for design iteration through simulations in the time domain. Since there are more complicated interactions with the feedforward and feedback torque inputs, multiple loops, and feedback loop transfer functions, it was decided that the feedback compensator should be designed using time domain

simulations with the full control system in operation. Therefore, all components of the control system were included for the design of the feedback compensator. Indeed, the feedback controller is not designed separately here because it has the twofold purpose of compensating for the residual tracking error from the feedforward torque input and the attenuation of the disturbance signal. Therefore, the full control system is simulated and the feedback compensation parameters are determined from the response of the full control system.

3.6. Full Control System

The full control system block diagram is shown in Figure 3-22.

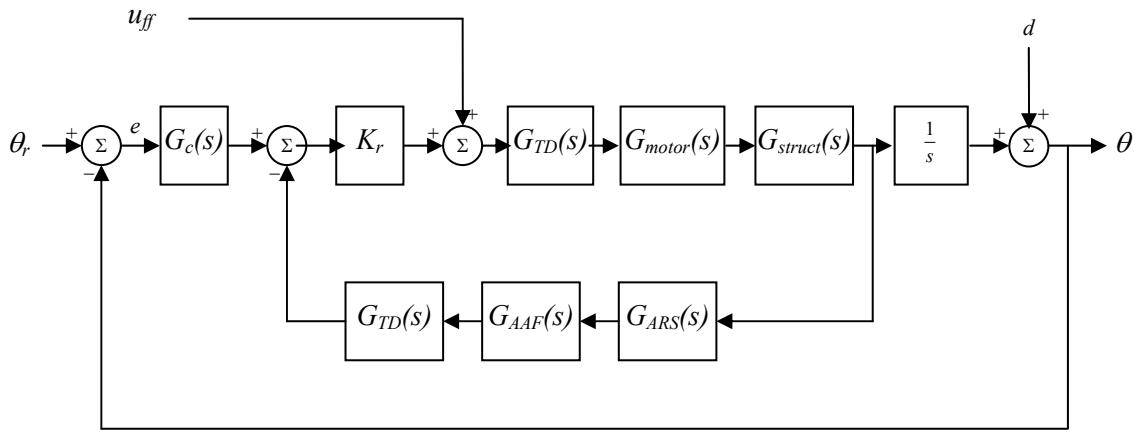

Figure 3-22: Full Control System Block Diagram

From Figure 3-22, it is seen that the slew angle is fed back to the compensator, $G_c(s)$. The antenna angle rate feeds through the sensor transfer functions in the feedback loop before it feeds back into the proportional gain compensator, K_r.

A simple lead compensator

$$G_c(s) = K_p \frac{s + p_c}{s + z_c} \tag{3-20}$$

is considered. From here, choosing the parameters becomes an iterative process. The gains K_r and K_p were evaluated based on their time response, and p_c and z_c were then adjusted so that the gains could be lowered.

The disturbance signal is now introduced. The disturbance signal is made up of a large number of tones ranging in frequency from about 0.1 to over 50 Hz. Each tone had its own amplitude and phase shift. The total disturbance signal is displayed in the figure below.

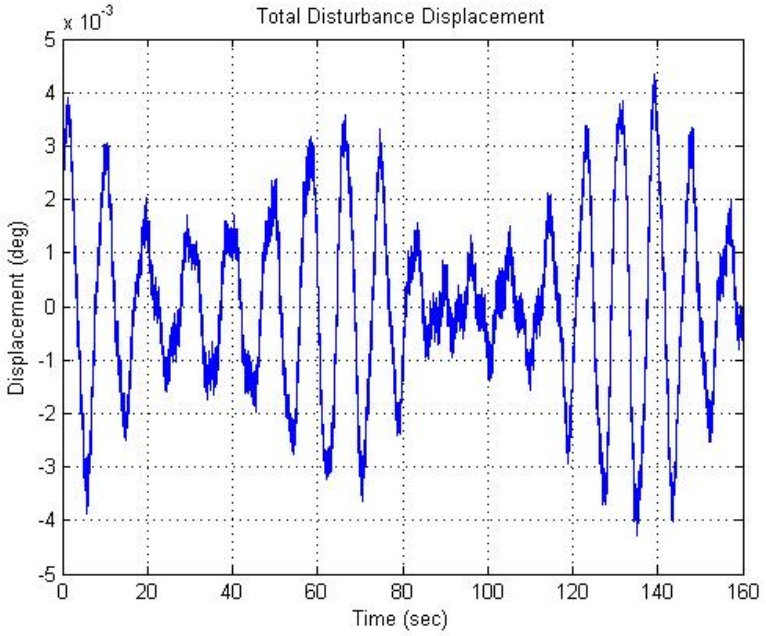

Figure 3-23: Pseudo-Random Disturbance Signal

The compensation parameters were varied until the disturbance transfer function peak frequency magnitude response was below -6 dB and the settled time response was within five microradians of the desired response. A slightly less significant issue was the speed of response. It is taken into consideration, but because the other two performance specifications are so tight, the speed of response does not appreciably vary once the other two specifications are met.

The final parameters for the compensator are listed below.

$$K_r = 50 \text{ oz} \cdot \text{in} \cdot \text{s}$$

$$K_p = 200 \text{ s}^{-1}$$

$$G_c(s) = \frac{K_p(s+1)}{s+5}$$

The time response and the frequency response of the disturbance transfer function are shown in Figures 3-24 and 3-25. Note the beneficial impact of feedforward action in Figure 3-24. There is no overshoot and the antenna slews one radian in six seconds, just as it was designed. In Figure 3-25 it is shown that feedback compensation attenuates the disturbance signal to -6 dB in the worst case. The open loop gain and phase margins are shown in Figure 3-26 to show the stability robustness. Note the tight slew angle steering performance. The time response is very close to the desired time response as shown in Figure 3-13.

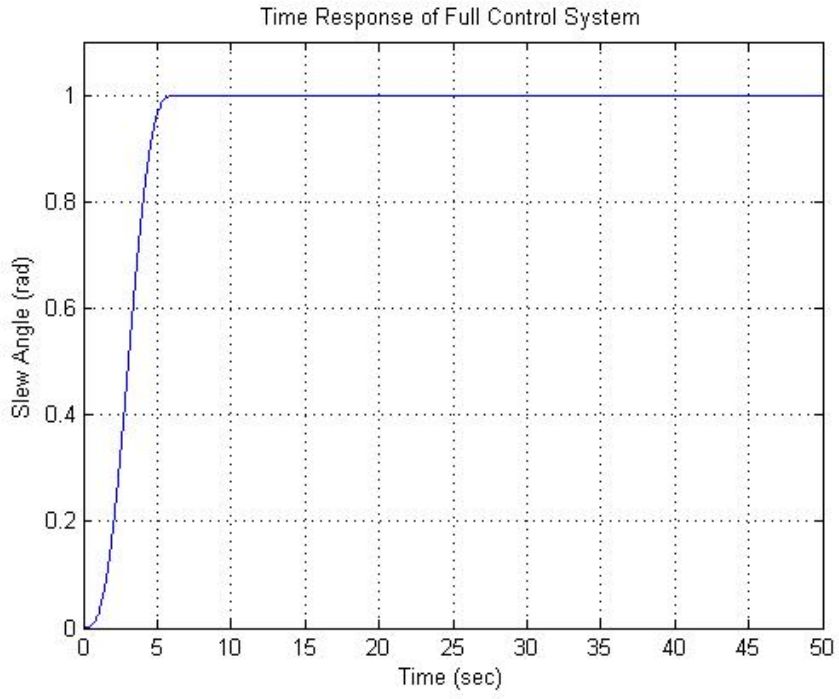

Figure 3-24: Slew Angle Response of Full Control System

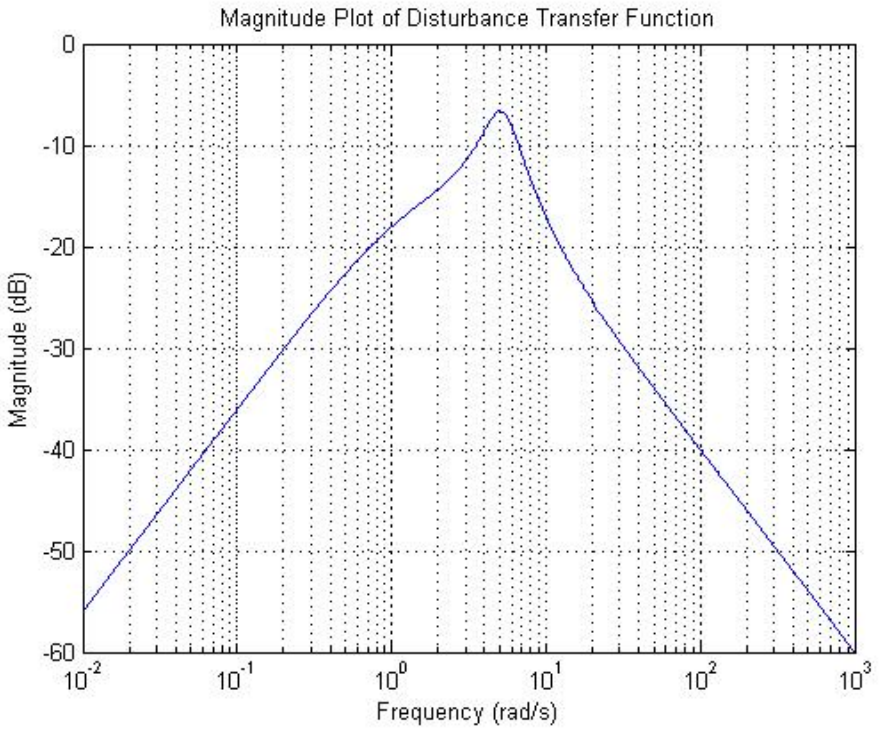

Figure 3-25: Bode Magnitude Plot of Disturbance Transfer Function

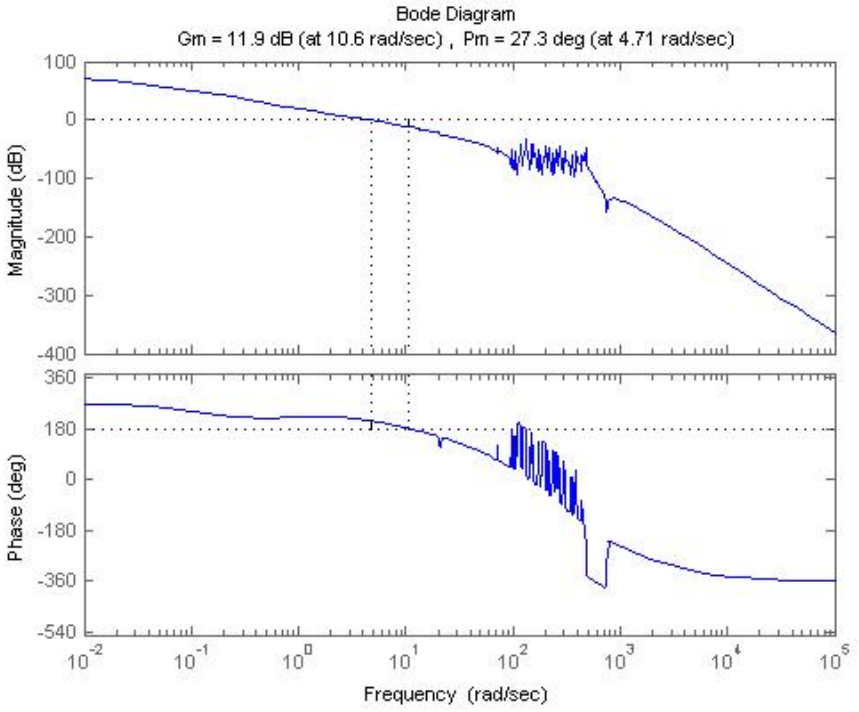

Figure 3-26: Gain and Phase Margins Compensated Control System

The control system meets all performance specifications. The comparison to the performance of the pure open loop system and pure feedback system to the integrated feedforward/feedback system is discussed in Chapter 4, as is the experimental proof that the uncertainty of the plant does not cause the performance specifications to be violated.

3.7. Experimentation with the Full Control System

Now that the full control system has been fully implemented, the validation of the design is outlined in this section. The first part of the experimentation is to prove that the integration of the feedforward and feedback control concepts provides a better response than the individual use of either. The second part of the experimentation proves the point that the high uncertainty in the plant and disturbance frequency range can place the controlled system outside of the performance specifications. Thus, the importance of reducing or bounding the uncertainty is underlined.

3.7.1. Comparison to Pure Feedforward and Feedback Control

The pure open loop control system is simulated in the presence of the disturbance signal. Since there is no feedback action in the open loop system, there should be no attenuation in the disturbance signal.

The feedback controller is simulated in the presence of the disturbance signal. Since the same feedback compensation scheme is used, the effects of the disturbance signal should be attenuated just as well, once the system reaches a steady-state. However, since there is no feedforward control, it is assumed that the feedback compensator will need to exert extra control effort to slew the antenna structure. Thus a

larger overshoot is expected, and some structural vibrations may be evident in the steady-state response.

3.7.2. Simulation of Plant Uncertainty

The plant transfer functions have several parameters which need to be estimated or determined by SYS ID. A number of these parameters may be difficult to determine and may easily vary, depending on the space environment of the plant.

It is assumed that the maximum variation of the plant parameters is ±10 percent of their nominal value. To analyze the effect of varying the plant parameters on the system response, critical plant parameters were altered by ±10 percent. This variation range is used because it is consistent with the parameter estimation performance of SYS ID. This variation is assumed to encompass the errors not only in SYS ID, but changes in parameter variation over time (e.g. aging). The specific parameters which are varied are chosen based on the difficulty of determining the parameter by SYS ID as well as the likelihood that the parameter will change over time.

This analysis is in the spirit of QFT, except here the reverse is done. In QFT the controller is designed based on the worst case scenario. In this investigation the worst case scenario is developed after the controller has been designed. The controller must meet all performance specifications in the worst case scenario before it can be considered robust enough for the uncertainty of the plant model.

The first parameters to be considered were the natural frequencies of the flexible modes. At high frequencies, most structures vibrate at small amplitudes when excited at their natural frequency. SYS ID measures free responses to determine the natural

frequencies; however, the measurements are corrupted by noise. Therefore, the frequency estimates can often be inaccurate. Also, due to fatigue and stress, the structural modes may change.

The second parameter taken into consideration was the modal peaks of each of the structural modes. These peaks represent the amplitude ratio of the output divided by the input of vibration of each mode. Without sufficient measuring equipment, the peaks determined by SYS ID will be miscalculated. Also, similar to the frequencies of structural modes, the modal peaks may change due to the stiffening or softening of the structure over time.

The third parameter taken into consideration was the moment of inertia of the rigid body model. Over the lifetime of the antenna this may change due to structure adjustments. The overall variation of the moment of inertia caused the disturbance magnitude maximum to increase in both directions; the minimum was of course at the nominal position.

The next parameter taken into consideration is the time delay. The time delay is due to the computational cycle time.

The next parameter that was varied was the amplifier bandwidth. The bandwidth is likely to change over the lifetime of the motor, mostly due to the degradation of the amplifier electronics in the space environment.

The last parameter that was varied was the motor gain. Essentially this constant acts as an amplifier as well, because it converts a current into a torque. This motor gain is likely to change over time, also, due to degradation of the hardware. Since it may vary

slowly over time, it is also difficult to determine solely based on an initial System ID experiment.

3.8. Chapter Review

This chapter covers the derivation of the feedforward and feedback control concepts used in this investigation. The feedforward control concept inputs a known torque signal to get the desired slewing response. The feedback compensator employs angular rate proportional gain feedback and angle feedback with lead compensation to meet the desired performance specifications.

This chapter also reviews the background of the experimentation covered in Chapter 4. The comparison of integrated feedforward and feedback control to the two separated control concepts is rationalized. Also the investigation of the effects of plant uncertainty is detailed.

IV. Results and Analysis

4.1. Control System Integration

There are two parts of the total control system, feedforward control and feedback compensation. In this section, it is shown that the integration of the two yields a better time response than each of them would individually.

Figure 4-1 shows the open loop control scheme. The feedback portion of the fully integrated control system is removed. There is no way for this controller to attenuate the disturbance signal since there is no feedback control action.

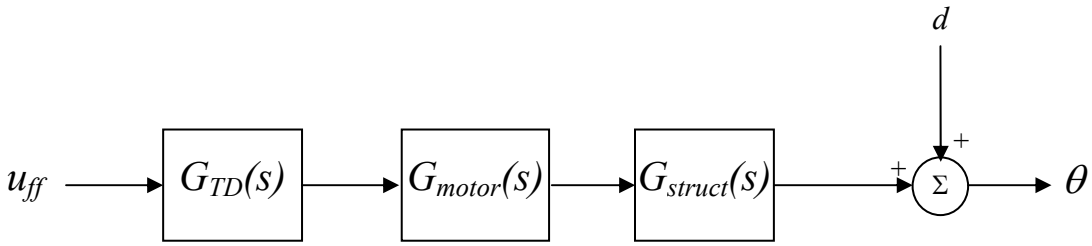

Figure 4-1: Open Loop Control

Figure 4-2 shows the feedback compensation scheme. Here, the feedforward control input is removed. However, there is feedback action, so the disturbance attenuation should be approximately the same. However, since there is no feedforward control, the feedback control action needs to be much greater in order to also perform the slewing control task; therefore, a more oscillatory response is expected.

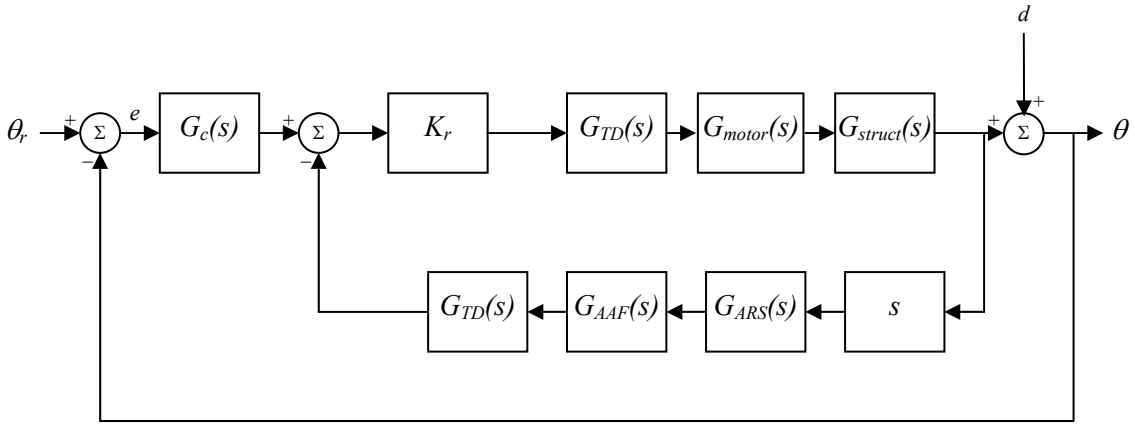

Figure 4-2: Feedback Compensation

The time responses of the open loop control, the feedback compensation, and the integrated control system are shown in Figure 4-3. As expected, there is a much larger overshoot in the time response of the feedback compensator. The result is that it takes much more time for the response to settle. Also as expected, there is no disturbance attenuation in the time response produced by the feedforward controller alone. This is unacceptable because the slew angle never stays within the performance specification's accuracy bounds.

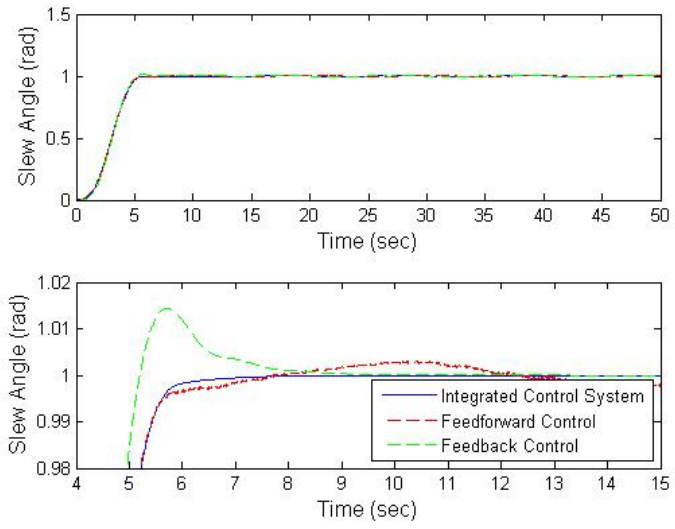

Figure 4-3: Time Domain Response of Feedback, Feedforward, and Integrated Control

Figure 4-3 proves that feedback control is essential to disturbance attenuation and that the performance specifications can not be met without it. Figure 4-4 shows the absolute value of the errors between the three responses and the desired response presented in Figure 3-13. The overshoot in the feedback compensator is shown here and the feedforward compensation error is just the absolute value of the disturbance signal, since there is no attenuation.

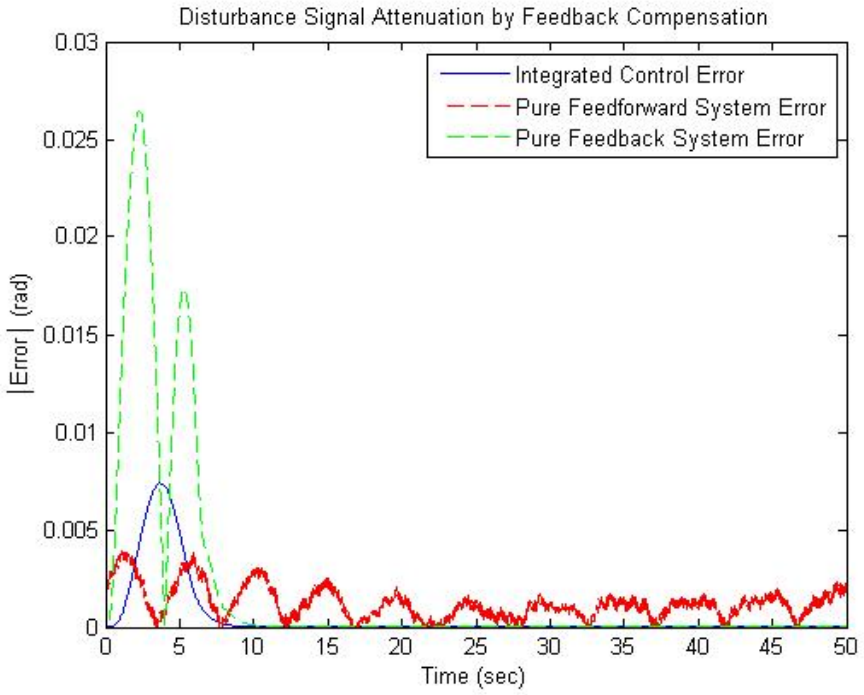

Figure 4-4: Errors between the Time Response and Desired Response

Figure 4-5 is a closer look at the errors on a microradian scale since they can not be seen in Figure 4-4. It is seen here that after about fifteen seconds the two compensators match up very closely. The advantage of the integrated control system is that a smaller overshoot ensues with the same amount of gain. In order for the pure feedback compensator to respond with the same amount of overshoot, the gains would need to be increased.

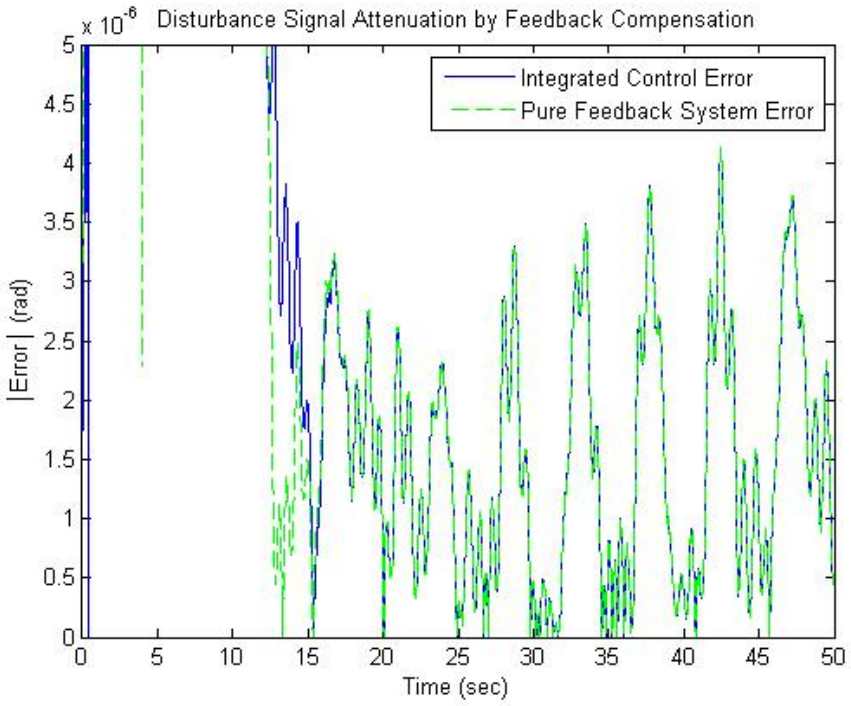

Figure 4-5: Errors in the Time Response (Feedback and Integrated Control Only)

A close-up view of the Bode Magnitude plot shown in Figure 3-25 is presented here. The highest point that the disturbance transfer function reaches is -6.624 dB. This is of course below the 6 dB specification. This specification insures that in the worst case scenario where a disturbance tone has the exact frequency where the magnitude was the greatest, the feedback controller can still attenuate the effect of the disturbance on the antenna pointing angle by a factor of 4.

It is shown that the fully integrated control system meets the disturbance attenuation performance specification of -6 dB attenuation and the accuracy performance specification of ±5 microradian accuracy. It is also shown that the fully integrated control system yields a better time response than the individual control components. Thus, the utility of integrated feedback and feedforward control is proven for the nominal plant.

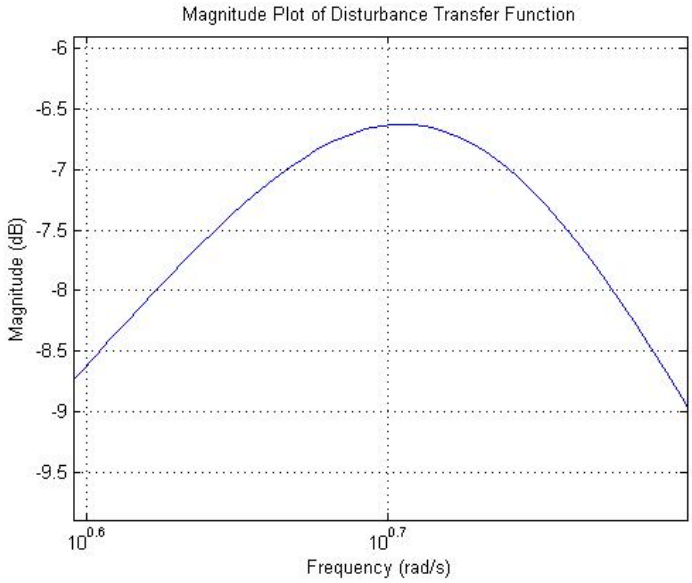

Figure 4-6: Maximum Value Disturbance Bode Magnitude Plot with Full Compensation

4.2. Proof of Performance with Plant Uncertainty

This section shows the time and frequency domain changes as critical plant parameters are varied from their nominal values. Again, each parameter is assumed to be accurate to within ten percent of its nominal value. This uncertainty encompasses all error sources.

4.2.1. Variation of Structural Modes Natural Frequencies

Each flexible mode's frequency was altered by ten percent from its nominal value. The resulting changes in the nominal plant are more evident in the time domain. The disturbance sensitivity in the frequency domain remained virtually unchanged with a change in structural frequency. However, the errors in the time domain show that when the structure modes are decreased, the errors slightly increase. The error changes are

typically on the order of 10^{-8} radians. However, as the structural mode frequencies decreased there is a consistent increase of the errors in the time domain across the entire time response of the control system.

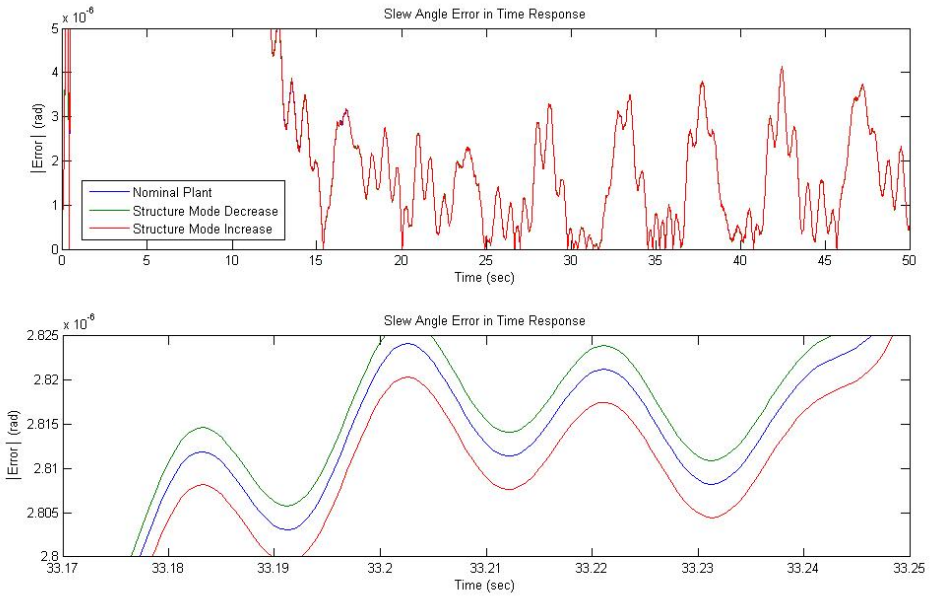

Figure 4-7: Time Domain Errors with Structure Natural Frequency Variation

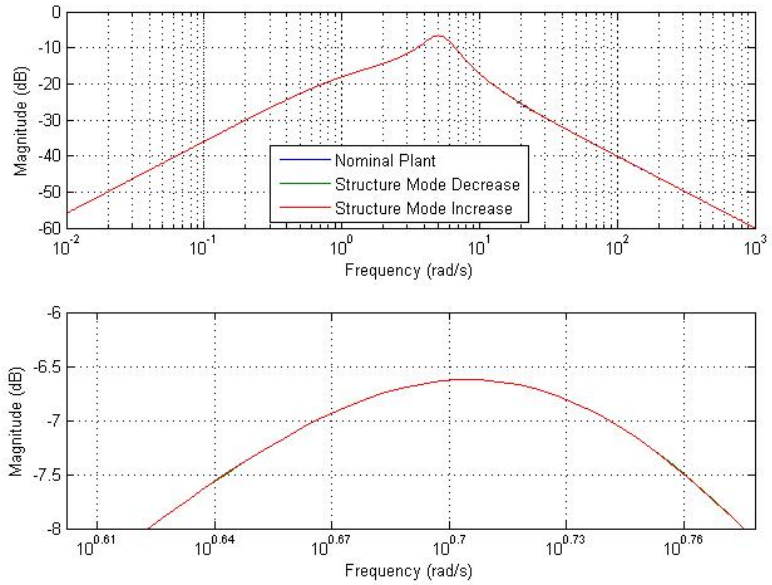

Figure 4-8: Disturbance Transfer Function Magnitude when the Structure Natural Frequencies Vary

4.2.2. Variation of Structural Modal Peaks

In the time response, the change in errors with a ten percent variation is much smaller than it was when the structure frequencies were varied. Again, there is virtually no change in the disturbance signal attenuation when the modal peaks are varied. The time response errors increase very slightly for a ten percent increase in modal peak values. For all intents and purposes, the variation of this parameter can be considered to have a negligible effect on the performance of the control system. This is somewhat expected since the effects are small and only applicable in the high frequency range where all the flexible structure modes are.

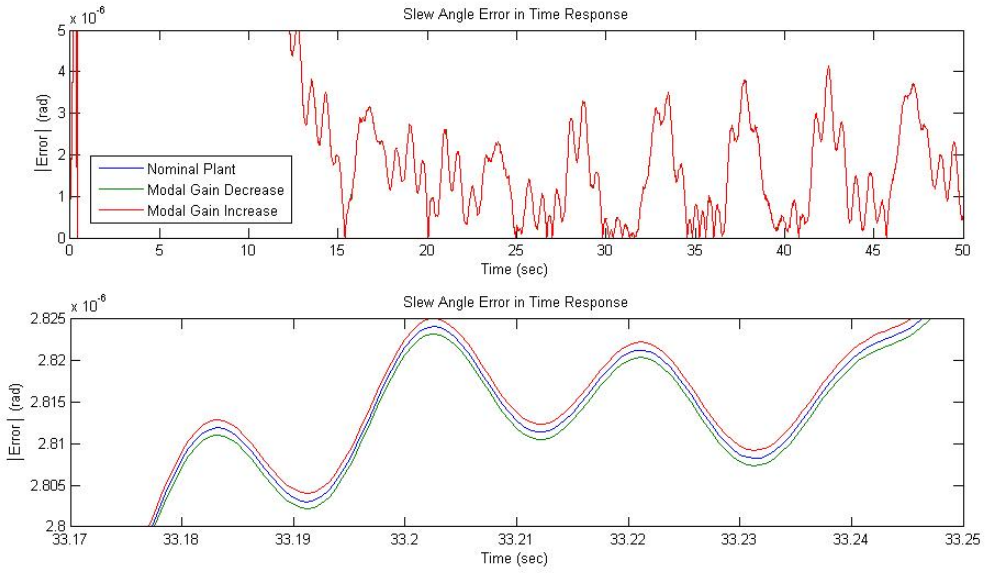

Figure 4-9: Time Domain Errors with Structure Modal Peak Variation

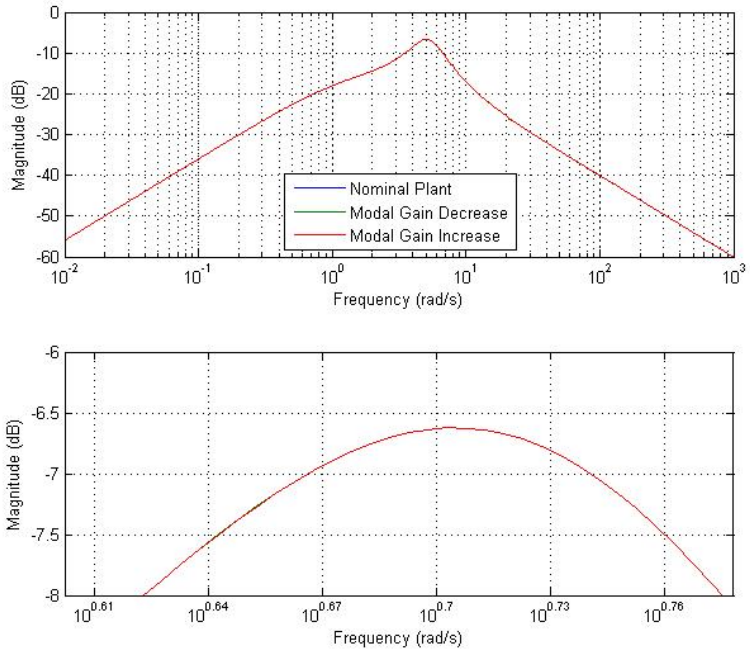

Figure 4-10: Disturbance Transfer Function Magnitude with Modal Peak Variation

4.2.3. Variation of Rigid Body Moment of Inertia

The variation in the rigid body moment of inertia caused the frequency response disturbance magnitude maximum to increase slightly in both directions. The moment of inertia also had a significant impact on the frequency at the peak disturbance sensitivity transfer function magnitude. A moment of inertia increase generally caused an increase in the time domain errors. This is expected because the increase in inertia would make it more difficult for the motor to dampen out the vibrations.

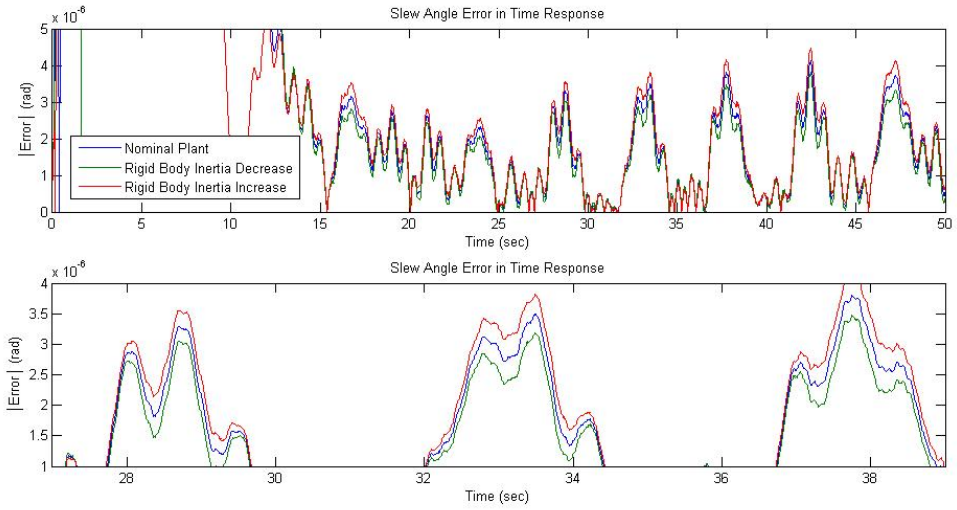

Figure 4-11: Time Domain Errors with Rigid Body Moment of Inertia Variation

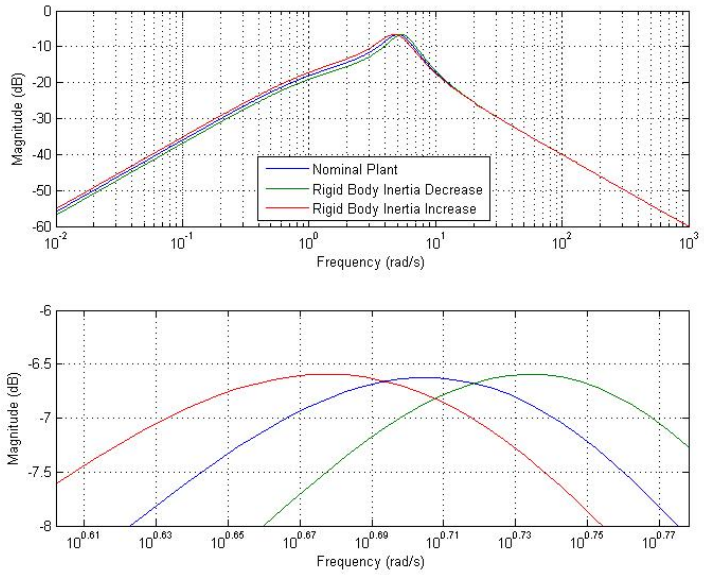

Figure 4-12: Disturbance Transfer Function Magnitude with Moment of Inertia Variation

4.2.4. Variation of Time Delay

The variation in time delay only extended for one millisecond in each direction. However, this has had the largest effect on both the time and frequency response of the system seen thus far. In some time periods the largest errors occurred when the time

delay increased, and in other time periods the largest errors occurred when the time delay was decreased. In the frequency domain, a one millisecond increase in time delay increased the maximum magnitude from -6.624 dB to -6.52 dB. While this is still well below the -6 dB specification, it shows the magnitude of the impact of the time delay on the performance of the controls system.

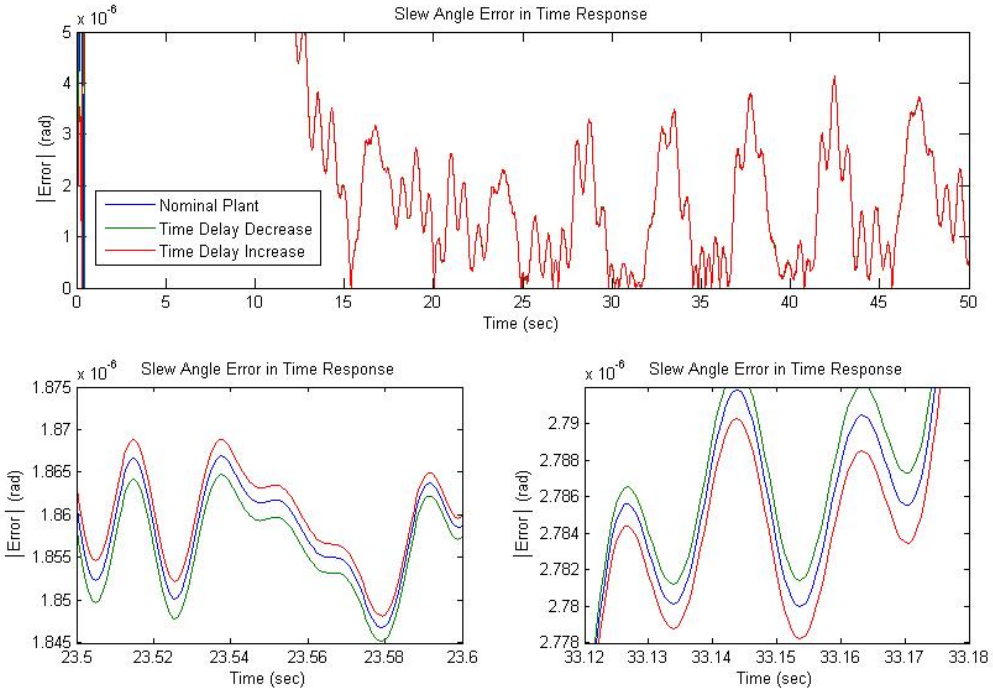

Figure 4-13: Time Domain Errors with Time Delay Variation

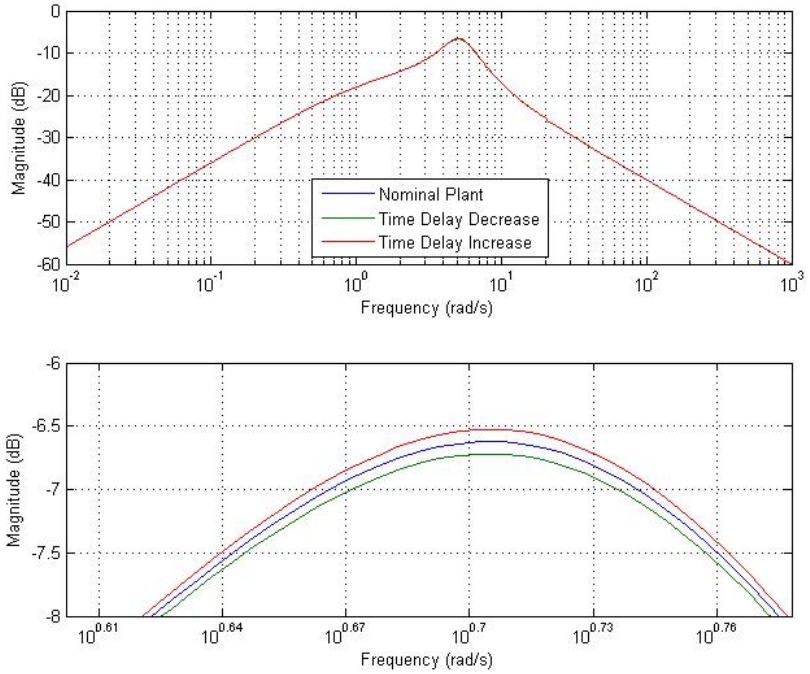

Figure 4-14: Disturbance Transfer Function Magnitude with Time Delay Variation

4.2.5. Variation of Amplifier Bandwidth

As the bandwidth of the amplifier decreased, so did the disturbance attenuation. The time domain errors were negligible and no particular trend is discernible. The change in bandwidth resulted in a very large increase in the disturbance sensitivity magnitude. With a bandwidth frequency decrease of ten percent, the disturbance magnitude increases to -6.44 dB. This parameter is also very critical because small changes result in a high impact on performance in the frequency domain.

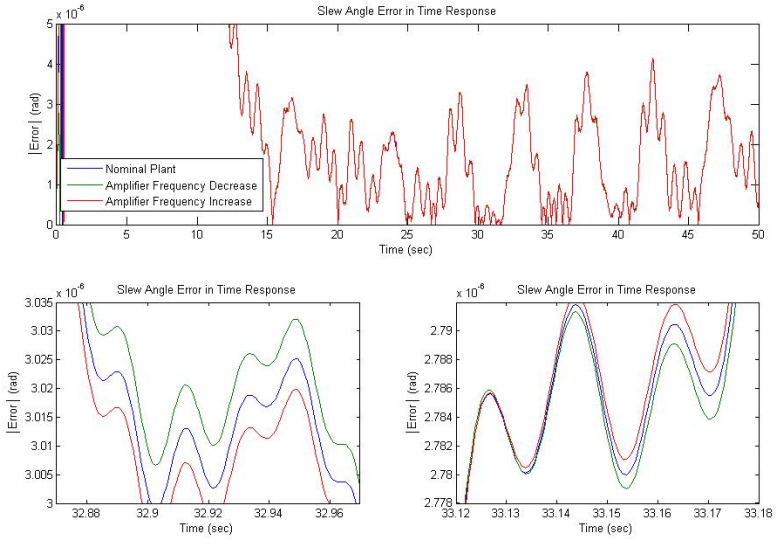

Figure 4-15: Time Domain Errors with Motor Bandwidth Variation

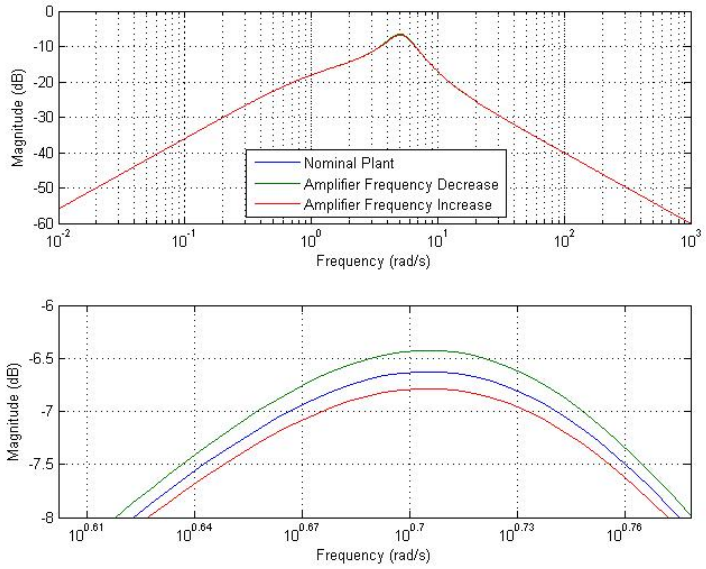

Figure 4-16: Disturbance Transfer Function Magnitude with Motor Bandwidth Variation

4.2.6. Variation of Motor Constant

When the motor gain was varied, the disturbance maximum followed a parabolic shape as was the case when the rigid body moment of inertia was changed. The more

significant change in the frequency response was the change in the frequency of the maximum disturbance sensitivity. The frequency of the maximum increased as the motor gain increased. However, the time domain errors increased significantly when the motor constant was decreased.

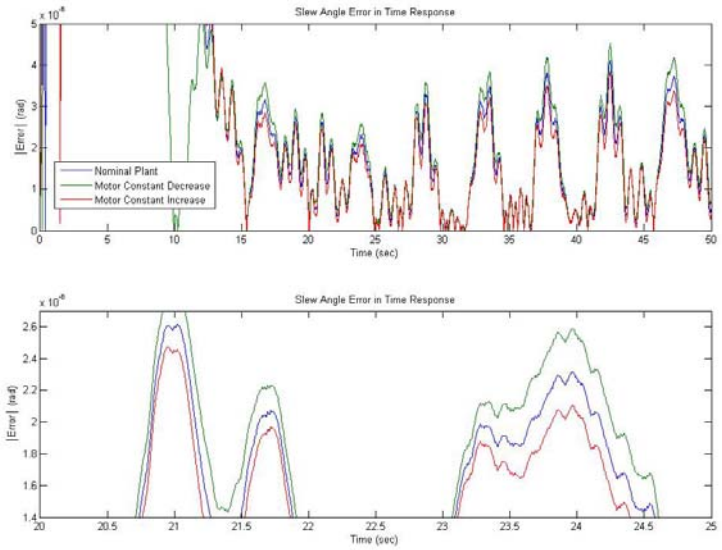

Figure 4-17: Time Domain Errors with Motor Gain Variation

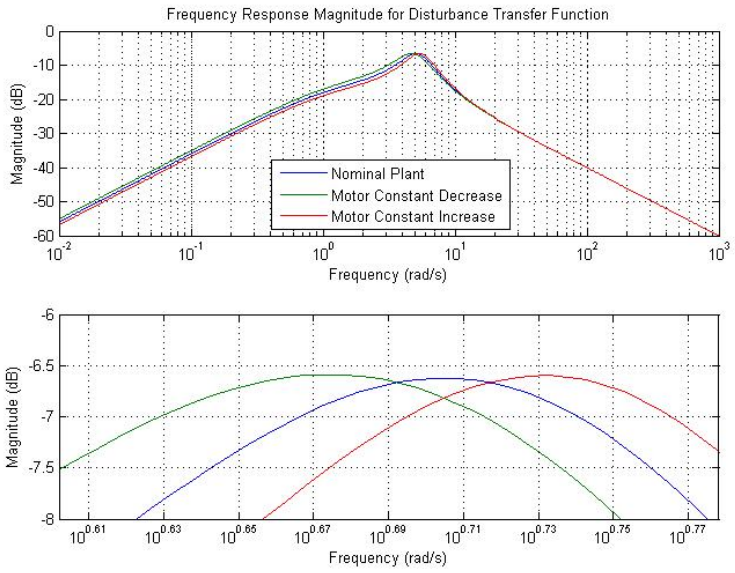

Figure 4-18: Disturbance Transfer Function Magnitude with Motor Gain Variation

4.2.7. Summary of Sensitivity Study

The following table summarizes the effects of the critical plant parameter variations on the time and frequency response. Most variations had better performance in one direction and worse in another. The rigid body moment of inertia and the motor gain variations caused a more parabolic curve, where the best response resulted when the variation was zero.

Parameter	Time Domain (90%)	Frequency Domain (90%)	Time Domain (110%)	Frequency Domain (110%)
Structure Mode Freq.	Larger Error	Negligible	Smaller Error	Negligible
Modal Peak	Negligible	Negligible	Negligible	Negligible
Moment of Inertia	Negligible	Parabolic Decrease	Negligible	Parabolic Decrease
Time Delay	Inconclusive	Smaller Maximum	Inconclusive	Larger Maximum
Motor Bandwidth	Inconclusive	Larger Maximum	Inconclusive	Smaller Maximum
Motor Gain	Larger Error	Parabolic Decrease	Smaller Error	Parabolic Decrease

Table 4-1: Summary of Variation Impacts on Frequency and Time Domain Responses

Figure 4-19 shows how the maximum magnitude of the disturbance sensitivity transfer function changed with the critical parameter variations. The largest impacts on the magnitude are from the time delay and the amplifier bandwidth. Thus, these two parameters are the most critical to bound so that the uncertainty remains low.

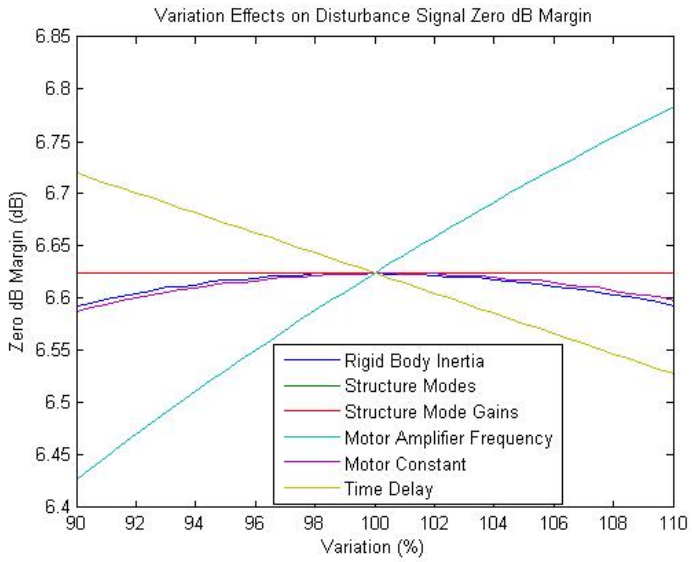

Figure 4-19: Individual Parameter Variation Effects on Disturbance Margin

4.3. Worst Case Scenario

4.3.1. Justification of the Worst Case Plant

The critical plant parameters were varied individually to see the effects on the time and frequency domain response. However, very rarely is the "worst case" scenario only going to involve the variation of a single plant parameter. In light of this, the previous analyses were used and simulations were performed to find the "worst case" scenario. Figure 4-19 graphically shows the effects of the variations of the individual parameters and assists in the determination of the worst case plant.

From the previous analyses, the time errors are well within the five microradian precision range. The disturbance rejection margin however, is very sensitive to many of the plant parameters, especially the time delay and motor bandwidth. Thus, in following the trends shown in Figure 4-19 of the disturbance margins, the variations are chosen based on the lowest disturbance rejection/margin of each individual parameter. The idea

being, that the combination of all the individual parameters would, in fact, be the overall worse case scenario. The table below shows the worst case scenario in the frequency domain, that is, the worst disturbance attenuation while each parameter was varied.

Parameter	Margin at 90%	Margin at 110%	Worst Case (FR)
Structure ω_n	6.624	6.624	Inconclusive
Modal Peaks	6.624	6.624	Inconclusive
Amplifier Frequency	6.438	6.784	90%
Motor Constant	6.588	6.598	90%
Time Delay	6.72	6.528	110%
Moment of Inertia	6.592	6.593	90%

Table 4-2: Table of Parameter Variations

The worst case scenario can not be determined only from this table. The variations in the first two parameters show inconclusive results. The frequency shift of the disturbance magnitude plot over the variations of the moment of inertia and motor gain should also be considered. Over several iterations it was determined that the worst case scenario occurred with the following parameter variations.

Parameter	Variation
Structure ω_n	90%
Modal Peaks	90%
Amplifier Frequency	90%
Motor Constant	90%
Time Delay	110%
Moment of Inertia	90%

Table 4-3: Worst Case Plant Variation

4.3.2. Response of Worst Case Plant

In this worst case scenario the maximum value of the disturbance magnitude response was -6.327 dB. There is still a margin of 0.327 dB before the system does not meet performance specifications. The time response errors are still well below the 5 microradian accuracy bounds, which is good.

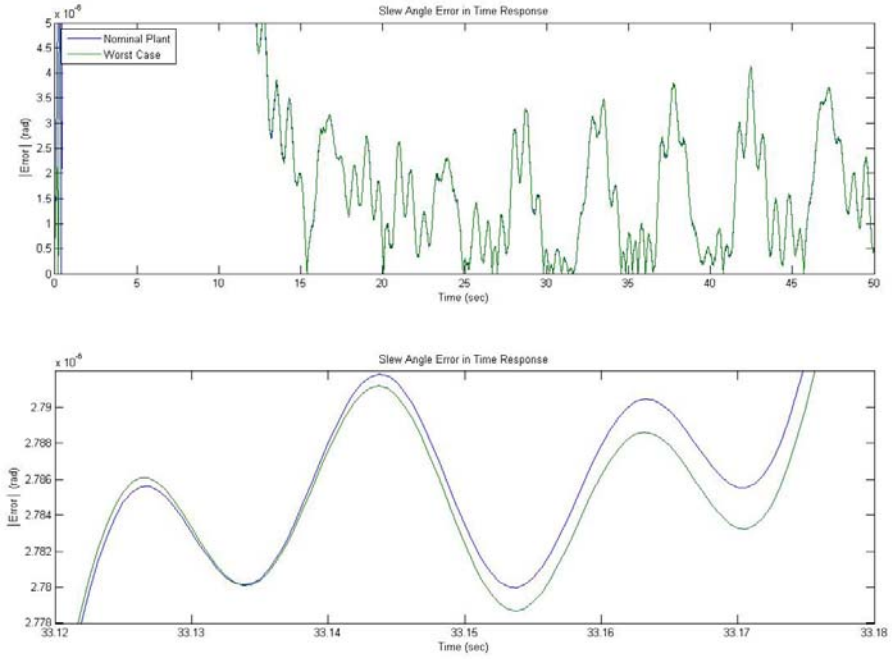

Figure 4-20: Time Domain Errors with Worst Case Plant

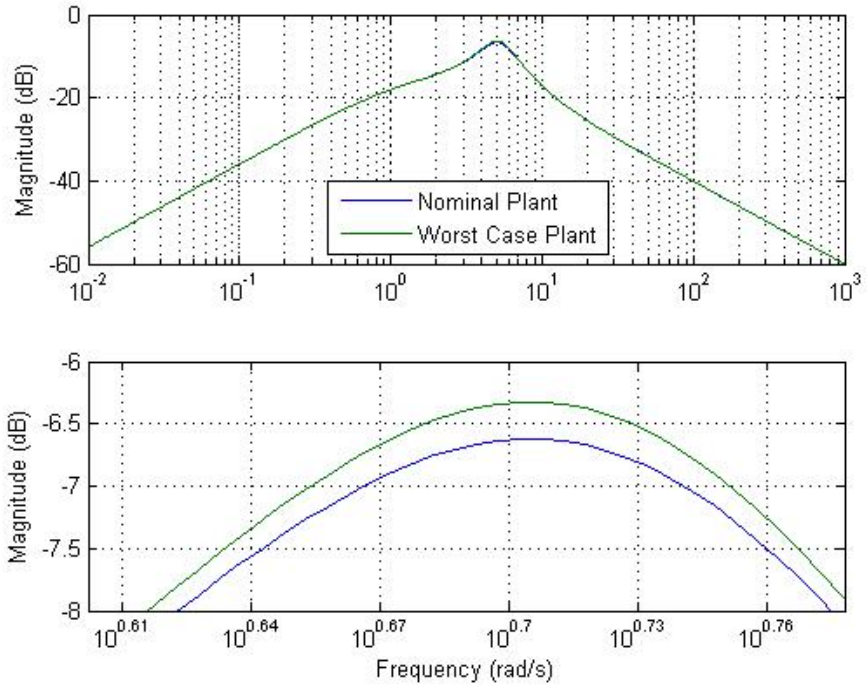

Figure 4-21: Frequency Response of Disturbance Magnitude with Worst Case Plant

4.3.3. Correcting the Compensator Gains

If the uncertainty of the parameters were absolutely bounded at ten percent, then the gains of the controller could be reduced to make the control system barely meet performance specifications. The following values of K_r and K_p still satisfy the performance specifications:

$K_r = 45\ oz{\cdot}in{\cdot}s$

$K_p = 180\ s^{-1}$

The new compensator parameters give a disturbance margin of 0.3 dB, which is slightly worse than the old controller, but the time errors are barely within the five microradian band of accuracy. The new values are a ten percent reduction of the original gains, thus a ten percent reduction in control effort. This also entails a ten percent reduction in electrical power used for control. This then underlines the importance of establishing the uncertainty bounds of different plant parameter estimates provided by SYS ID.

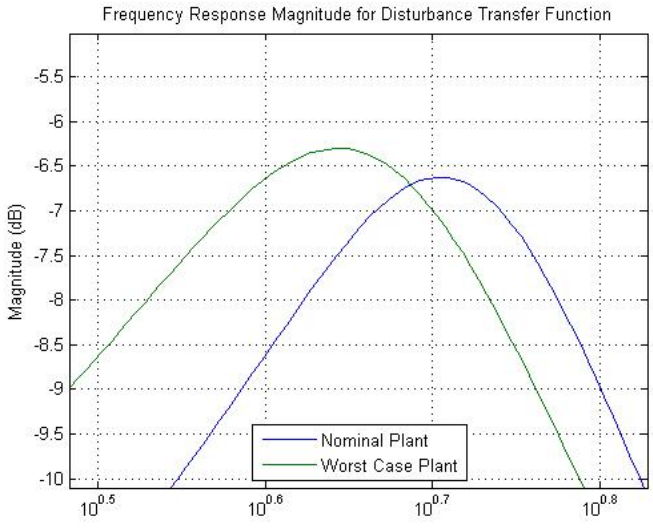

Figure 4-22: Lower Gain Disturbance Magnitude Maximum

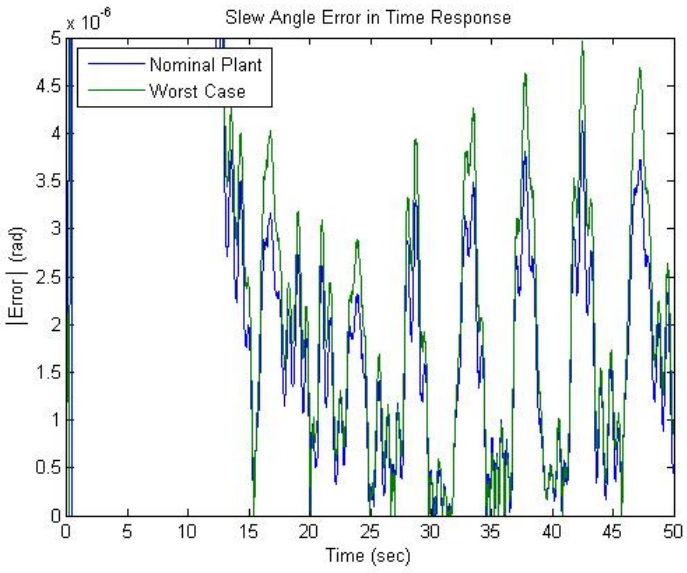

Figure 4-23: Time Response Errors with Lower Controller Gains

4.4. Summary of Results

The results presented in the beginning of this chapter show that an integrated control system does indeed perform better than pure feedback and pure feedforward control. It incorporates the disturbance attenuation capability of feedback control with the simplicity of open loop feedforward control to reduce the feedback control action.

The results presented in this chapter also prove the importance of bounding the uncertainty in the parameter estimates provided by SYS ID. With the error bounded at ten percent the gains could be reduced by 10 percent. If the error were any greater, it is likely that the same compensator gains would violate the performance specifications of the antenna plant.

V. Discussion and Conclusions

5.1. Concluding Remarks

The design of a robust controller for an uncertain antenna plant on board a spacecraft is considered in this paper. The performance specifications for the controller are 5 microradians steady-state accuracy and in the presence of an external disturbance signal the magnitude of the disturbance frequency response must be below -6 dB for the entire frequency band of the disturbance signal which is roughly between 0.1 and 50 Hz.

Sensor noise was not taken into consideration in this investigation. Noise effectively limits the amount of disturbance attenuation achievable because, in view of Equation 1-2, the high gains in the controller which are responsible for attenuating the disturbance will simultaneously amplify the sensor noise. The internal disturbances, of type d_1, were also disregarded in this investigation. Internal disturbances would normally come from actuation disturbances (i.e. motor recoil or dead zone). A separate d_1 disturbance signal would need to be included to model that type of disturbance, and the feedback compensator would need to attenuate that signal as well. Finally, the forward loop gains are capped by actuator saturation; that is, the maximum torque output of the motor. Since saturation limits were not available during this investigation, they were ignored. Having them available would be beneficial in determining an optimal control system.

Cognizant of sensor noise amplification and actuator saturation, the gains have been kept as low as possible while still satisfying the performance specifications of control accuracy and wideband disturbance rejection.

Specifically, the concept of utilizing feedforward control in conjunction with feedback compensation was thoroughly investigated. The feedback compensator is responsible for attenuating the disturbance signal, mitigating the deleterious effects of plant uncertainty, as well as mitigating any residual vibrations induced from the feedforward control signal. When combined with feedforward control, less feedback control action s needed to slew the antenna structure, since the model-based designed feedforward control input accomplished most of the slew maneuver. Since this was the case, the gains of the compensator could be reduced while still achieving a very precise slew maneuver, since less control effort is required from the compensator to slew the antenna.

At the conclusion of the design portion of the investigation, the controller is exercised in simulations with variations in plant parameters. The variations typically increased the amount of error in the signal and the magnitude of the disturbance sensitivity function. Thus, changes in the plant parameters away from the nominal often led to worse responses. A worst case plant was then created based on the patterns seen in varying different parameters. It was found that the performance of the controller, even given the worst case plant, exceedingly met the performance specifications. Therefore the gains were reduced by ten percent and the performance specifications were met. This underlines the importance of bounding uncertainty. If the uncertainty would be reduced more than ten percent, the gains could likely be further reduced.

5.2. Implications of Investigation

This investigation has given some insight to how the integration of feedforward action with feedback compensation can reduce the gains in the compensator. This avoidance of high gains is beneficial to avoid actuator saturation and to limit the sensitivity to sensor noise in the system. Also, the concept of plant uncertainty is addressed in this investigation. The ability to bind the certainty of the plant becomes crucial in high accuracy control applications. Research in this direction will only facilitate the spacecraft control applications.

5.3. Further Research

This investigation covered a narrow band of possibilities in both plant uncertainty and control implementation. In lieu of this, no serious effort was made in this investigation to "optimize" the response of this problem. Different applications of feedforward control can be studied. For example some the input torque shaping techniques discussed in Chapter 2 can be used in place of a single sine wave input. Also additional feedback compensation techniques can also be attempted to further lower the compensator gains. Better knowledge of the plant limitations (i.e. saturation limits, slew angle limits), as well as an applicable noise model would make further investigation in this direction more feasible.

In addition, System Identification techniques can also be studied to lower the range of uncertainty in the plant model. This research is guided more towards the study of individual system components. Therefore, the issue here becomes how to relate the experimental data to the parameters of the system components. Additionally, how

accurate are the system components to begin with. For example, if the motor exhibits behavior or dynamics not seen in the frequency response.

There are a number of different research directions available from the conclusions of this investigation. The most important are the investigation of system identification techniques and limitations and the investigation of new control concepts to optimize the time or frequency response of the system.

Appendix A. Nominal Plant Model

A.1. Plant Model Block Diagram

The actual spacecraft mounted antenna model used in this investigation is presented in transfer function form provided by the sponsor in a MatLab script file. The provided model is used as the nominal plant. It is assumed that the provided plant model is the creation of a SYS ID process. This model is assumed to be what the plant is, even though the plant parameters provided still remain – to some degree – uncertain.

The entire plant in block diagram form is shown in Figure A-1, where $G_{TD}(s)$ is the time delay transfer function located in the forward and feedback paths, $G_{motor}(s)$ is the motor transfer function, $G_{struct}(s)$ is the structure transfer function, $G_{ARS}(s)$ is the angle rate sensor transfer function, and $G_{AAF}(s)$ is the anti-aliasing filter transfer function.

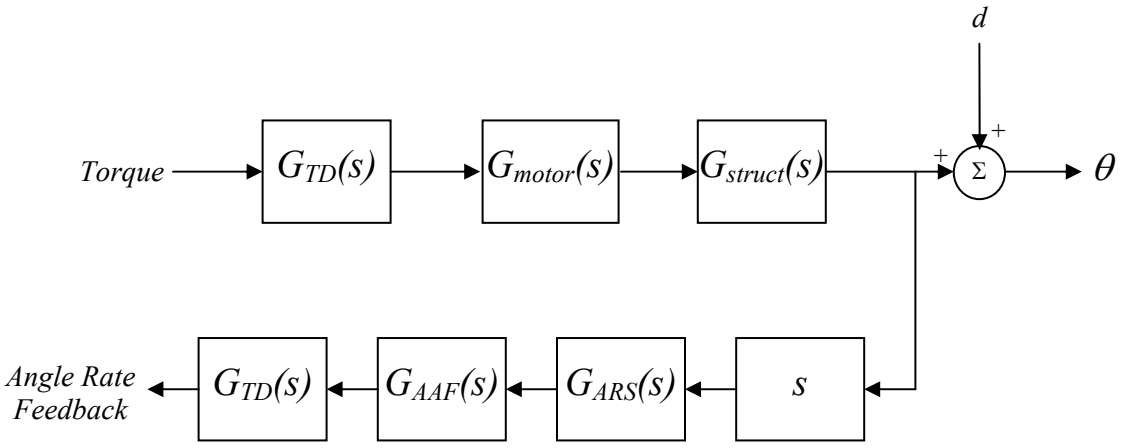

Figure A-1: Actual Plant Model Block Diagram

A.2. Structure Transfer Functions

The plant dynamics are given in transfer function form. There are several individual components of the plant model, and each component has its own transfer function. This sub-section explains each component and its transfer function.

The bare structure provided is characterized by the natural frequencies of 20 modes (ω_n), and their corresponding damping ratios (ζ) and modal peaks (k). Also included in the bare structure is the rigid body mode. Given the above values and the following equations, a linear model of the entire structure is created.

$$G_{i\text{th flexible mode}}(s) = \frac{k_i s}{s^2 + 2\zeta_i \omega_{n,i} s + \omega_{n,i}^2} \tag{A-1}$$

$$G_{\text{rigid body}}(s) = \frac{1}{Js^2} \tag{A-2}$$

$$G_{\text{structure}}(s) = G_{\text{rigid body}}(s) + \sum_{i=1}^{20} \mathrm{G}_{\text{flexible mode, } i}(s) \tag{A-3}$$

In Equation A-2, J is the moment of inertia of the antenna's rigid body. From these equations, the bare space structure is modeled in a single transfer function. It is important to note that these transfer functions relate the torque input to the pointing angle of the flexible structure. Multiplying the transfer function by a derivative s relates the input torque to the slew rate of the antenna, which is measured by an onboard angle rate sensor.

The flexible mode parameters, k, ω_n, ζ are listed in Table A-1. Figure A-2 shows the Bode plot of the structure transfer function. Note the higher modal peaks in the 15-75 Hz frequency band.

Flexible Mode	k (rad/oz-in $\times 10^{-6}$)	ω_n (Hz)	ζ
1	-1.5597	3.3	0.02
2	0.0242	11.5	0.0025
3	0.0255	15.5	0.0025
4	0.0189	16.5	0.0025
5	0.0720	19	0.0025
6	0.2990	21	0.0025
7	0.0909	24	0.0025
8	0.0980	24.5	0.0025
9	0.0419	28	0.0025
10	0.1288	32	0.0025
11	0.0808	34	0.0025
12	0.0287	38	0.0025
13	0.0784	41	0.0025
14	0.1793	43	0.0025
15	0.0642	48	0.0025
16	0.0617	49	0.0025
17	0.0408	56	0.0025
18	0.01367	62	0.0025
19	0.0676	70	0.0025
20	-0.3620	76	0.0025

Table A-1: Structure Transfer Function Parameters

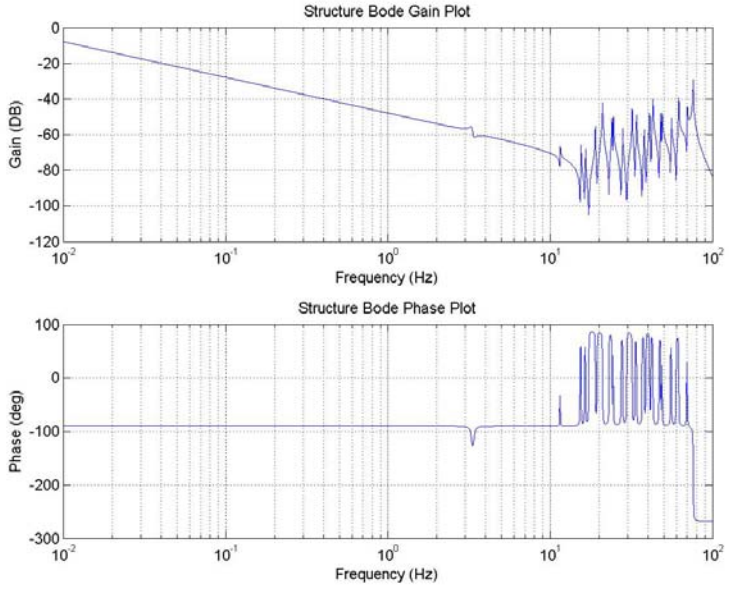

Figure A-2: Structure Bode Plots

A.3. Motor/Actuator Transfer Functions

The motor takes a commanded input torque and gives a smoother output torque to the structure. The motor/actuator has complicated dynamics. The components of the motor are the zero-order-hold, the amplifier, and the actuator. Their individual transfer functions are shown in Equations A-4 to A-6. The total motor/actuator transfer function is the product of the three.

$$G_{zoh}(s) = \frac{120000s}{s^3 + 600s^2 + 120000s} \tag{A-4}$$

$$G_{actuator}(s) = \frac{272.34375}{s + 2167} \tag{A-5}$$

$$G_{amplifier}(s) = \frac{52.47}{s + 53} \tag{A-6}$$

Figure 3-6 shows the Bode plot of the motor transfer function. Also included in the figure is the frequency response of a separate motor with a high gain amplifier. This motor has an amplifier modeled as a second order transfer function. For the purposes of this investigation, this motor is not used other than for open loop control experimentation discussed in Chapter 3. Therefore, its structure and parameters are not further discussed.

Note that the final value of the total low gain motor, that is its DC gain, is not equal to one. Thus, the motor does not track the commanded input. Therefore, the motor transfer function is multiplied by the inverse of $G_{motor}(0)$, such that 1 oz-in of input torque commanded will yield a steady-state output torque of 1 oz-in – see Equation A-7. This is consistent with conventional flight control actuators, which are typically first order filters of the commanded input with a DC gain of unity. This gain is especially important in the determination of the feedforward input torque signal – see Chapter 3.

$$G_{motor}(s) = k_m G_{zoh}(s) G_{actuator}(s) G_{amplifier}(s), \quad k_m = 8.037228 \tag{A-7}$$

A.4. Angle Rate Sensor Transfer Functions

The angle rate sensor tracks the output of the structure (angle rate) at low frequencies and attenuates the high frequency noise. Essentially, it is the relationship between the actual angle rate and the angle rate readings available for feedback, which, at high frequencies, may not match up. The transfer function is shown in Equation A-8.

$$G_{ARS} = \frac{1}{\left(\frac{s}{628.3}+1\right)\left(\frac{s}{680.2}+1\right)} \tag{A-8}$$

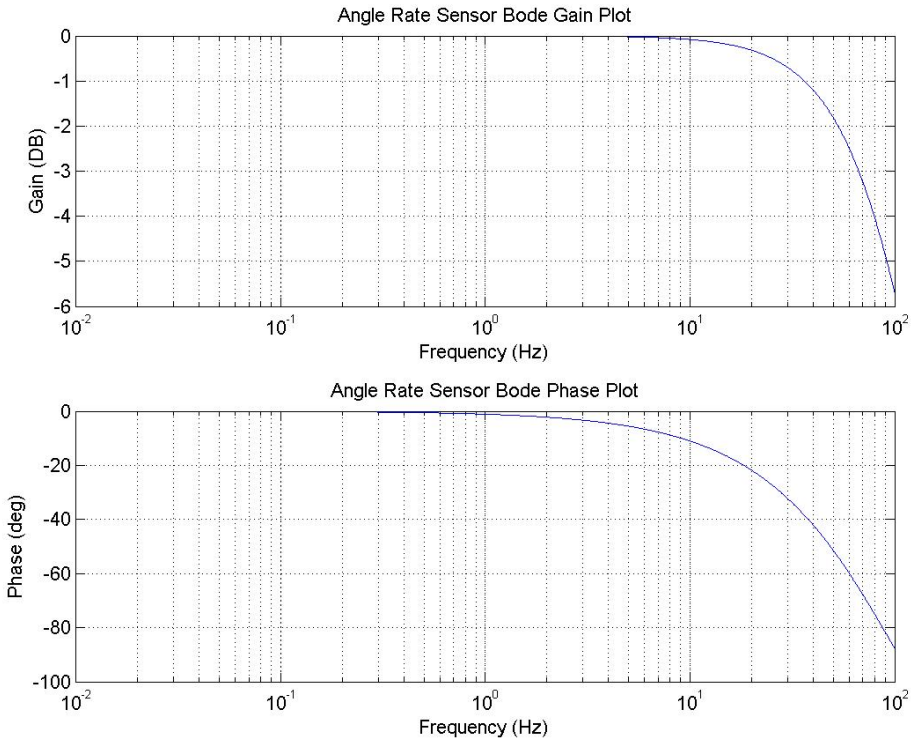

Figure A-3: Angle Rate Sensor Bode Plot

A.5. Anti-Aliasing Filter Transfer Function

The anti-aliasing filter restricts the bandwidth of the sensors' output so that the sensor data can be properly processed by the digital controller. From the transfer function below, it is evident that, the bandwidth of the anti-aliasing filter is 251.3 rad/s. Sensor data, mainly noise, of higher frequency will be attenuated by the filter.

$$G_{AAF} = \frac{251.3^2}{s + 2(0.707)(251.3)s + 251.3^2} \tag{A-9}$$

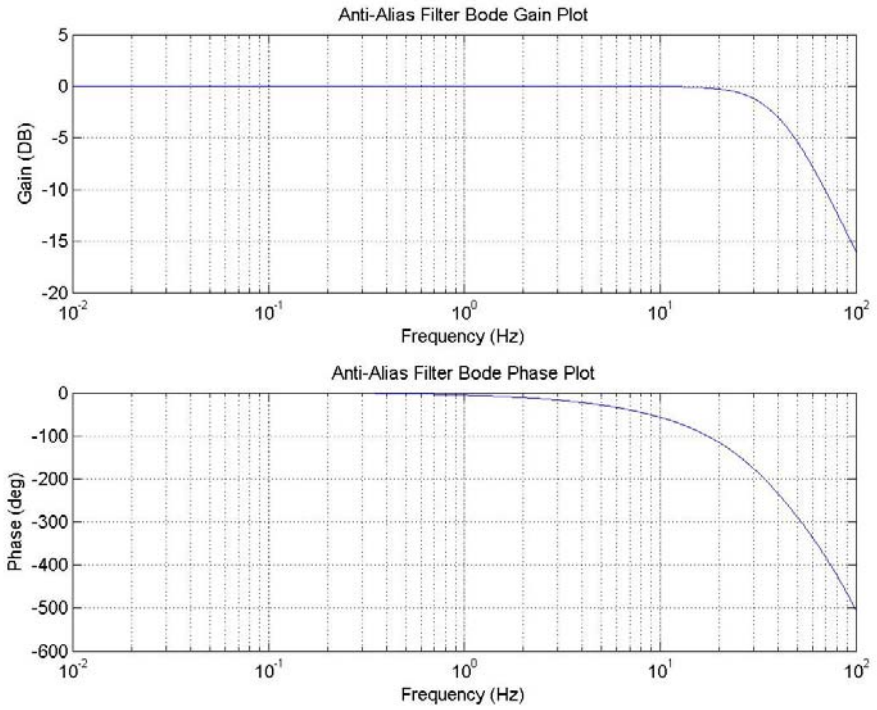

Figure A-4: Anti-Alias Filter Bode Gain Plot

Both the Anti-Alias Filter and the Angle Rate Sensor dynamics are low pass filters, with a limited bandwidth of roughly 30 Hz. Conveniently, their bandwidth is around the same order as the dominant dynamics of the structure. Therefore, care should be exercised not to utilize control inputs in the high frequency range.

A.6. Time Delays

There are an assumed two time delays present in the plant, one in the forward loop, and one in the feedback path. Both time delays are assumed to be 0.01 seconds. Whenever possible, the analysis of the Plant includes the true time delay transfer function, $e^{-0.01s}$. However, when the analysis did not allow the use of a pure time delay, the first order Pade approximation was used instead.

$$G_{TD}(s) = \frac{1 - 0.005s}{1 + 0.005s} \tag{A-10}$$

Appendix B. Basic Physics of Rigid Body/Flexible Appendage Models

A simple model was chosen to experiment with basic controllers to understand and predict the behavior of more complex models. This was done to understand the physics of the basic rigid body with a flexible appendage.

B.1. Derivation of Simple Plant Model

Before the actual plant model was considered, the antenna was assumed to have a center rigid body and a flexible appendage. To linearize the model, the appendage is considered to be made up of *n* inertial dumbbells; each inertial mass is attached to the next with torsional springs and dampers. The equations of motion for the model are similar to that of a translational *n* mass-spring-damper system. Refer to Figure 1-2 for an illustration. Rotational dynamics are similar in structure to translational dynamics, so as common with translational spring-mass-damper systems, the equations of motion are linearized and expressed in state-space with a state vector of physical states – see Equation B-1.

$$\dot{\bar{x}} = A\bar{x} + Bu \tag{B-1}$$

The equations of motion are derived as follows:

$$\sum M_0 = J_0\ddot{\theta}_0 \tag{B-2}$$

Here, J_0 is the moment of inertia of the center rigid body. M_0 is the moment about the longitudinal axis of the body. Consider the center rigid body equations of motion,

$$J_0\ddot{\theta}_0 = T - k_1(\theta_0 - \theta_1) - d_1(\dot{\theta}_0 - \dot{\theta}_1) \tag{B-3}$$

where θ_0 is the attitude of the rigid body, θ_1 is the attitude of the first element of the flexible appendage, T is the torque acting on the center mass, and k_1 and d_1 are the torsion spring and damping coefficients, respectively. Following this same pattern, the equations of motion for the first *n-1* elements that make up the appendage can be represented as:

$$J_i\ddot{\theta}_i = k_i(\theta_{i-1} - \theta_i) + d_i(\dot{\theta}_{i-1} - \dot{\theta}_i) - k_{i+1}(\theta_i - \theta_{i+1}) - d_{i+1}(\dot{\theta}_i - \dot{\theta}_{i+1}) \tag{B-4}$$

The n^{th} flexible element has the following equation of motion:

$$J_n\ddot{\theta}_n = k_n(\theta_{n-1} - \theta_n) + d_n(\dot{\theta}_{n-1} - \dot{\theta}_n) \tag{B-5}$$

Now, assuming the following equalities:

1) $k_1 = k_2 = \ldots = k_n = k$

2) $d_1 = d_2 = \ldots = d_n = d$

3) $J_1 = J_2 = \ldots = J_n = J << J_0$

Equations B-3, B-4, and B-5 yield:

$$J_0\ddot{\theta}_0 = -k\theta_0 - d\dot{\theta}_0 + k\theta_1 + d\dot{\theta}_1 + T \tag{B-6}$$

$$J\ddot{\theta}_i = k\theta_{i-1} + d\dot{\theta}_{i-1} - 2k\theta_i - 2d\dot{\theta}_i + k\theta_{i+1} + d\dot{\theta}_{i+1} \tag{B-7}$$

$$J\ddot{\theta}_n = k\theta_{n-1} + d_n\dot{\theta}_{n-1} - k\theta - d\dot{\theta}_n \tag{B-8}$$

Now, consider a column vector x, composed of physical variables of the system:

$$x = \begin{bmatrix} \theta_1 \\ \dot{\theta}_1 \\ \theta_2 \\ \dot{\theta}_2 \\ \vdots \\ \theta_n \\ \dot{\theta}_n \end{bmatrix}_{2(n+1)}$$

A state-space model with the state vector x can be constructed in the form shown in Equation B-1.

Using the definitions

$$\omega_0 \equiv \sqrt{\frac{k}{J_0}},\ \omega \equiv \sqrt{\frac{2k}{J}},\ \omega_n \equiv \sqrt{\frac{k}{J}}$$

$$\zeta_0 \equiv \frac{1}{2}\frac{d}{\sqrt{kJ_0}},\ \zeta \equiv \frac{1}{\sqrt{2}}\frac{d}{\sqrt{kJ}},\ \zeta_n \equiv \frac{1}{2}\frac{d}{\sqrt{kJ}},$$

$$H = \begin{bmatrix} 0 & 1 \\ -\omega^2 & -2\zeta\omega \end{bmatrix}, H_0 = \begin{bmatrix} 0 & 1 \\ -\omega_0^2 & -2\zeta_0\omega_0 \end{bmatrix}, H_n = \begin{bmatrix} 0 & 1 \\ -\frac{1}{2}\omega^2 & -\zeta\omega \end{bmatrix}$$

$$K = \begin{bmatrix} 0 & 0 \\ \frac{1}{2}\omega^2 & \zeta\omega \end{bmatrix}, K_0 = \begin{bmatrix} 0 & 0 \\ \omega_0^2 & 2\zeta_0\omega_0 \end{bmatrix},$$

the dynamics matrix, A, is a $2(n+1)$ square matrix and is obtained as shown below:

$$A = \begin{bmatrix} H_0 & K_0 & 0 & \cdots & 0 \\ K & H & K & \ddots & \vdots \\ 0 & K & H & K & 0 \\ \vdots & \ddots & \ddots & \ddots & K \\ 0 & \cdots & 0 & K & H_n \end{bmatrix} \tag{B-9}$$

Upon further evaluation of H_0, it can be assumed that $J_0 >> k$ and $J_0 >> d$. Effectively, this reduces H_0 to the matrix:

$$H_0 = \begin{bmatrix} 0 & 1 \\ 0 & 0 \end{bmatrix} \tag{B-10}$$

This approximation of H_0 yields two eigenvalues of the complete A matrix with the value of zero. This approximation makes sense, since H_0 models the rigid body portion of the structure. Physically speaking, a torque is commanded to the rigid body and the rigid body responds as an angle which is the second derivative of the commanded torque; hence, the two eigenvalues at zero.

A Bode plot of the simple model is shown in Figure B-1. The model approximated the appendage as 30 inertial masses.

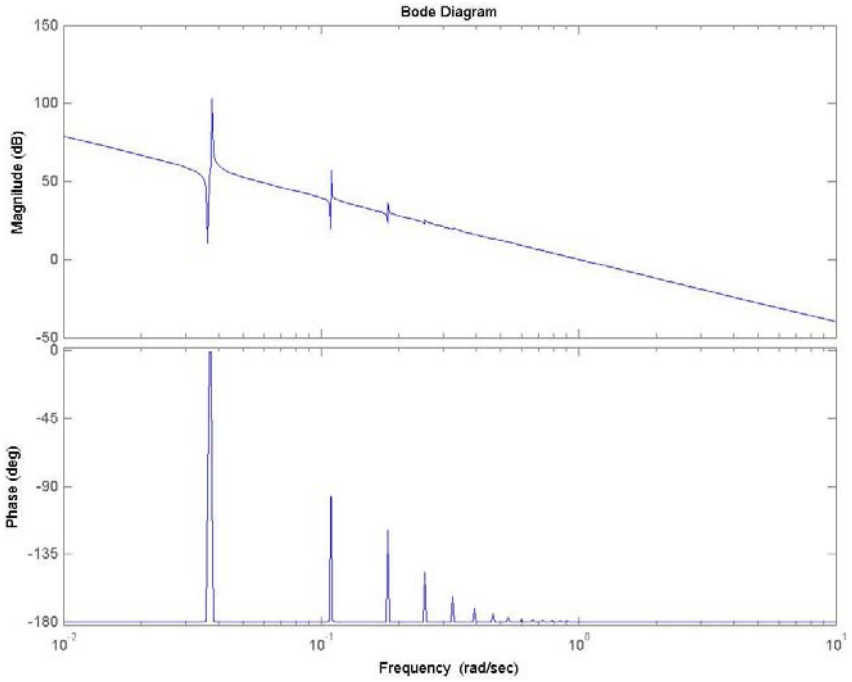

Figure B-1: Bode Plot of Simple Plant Model

The Bode diagram shows that all of the prominent dynamics of the model occur at frequencies less than 1 rad/s. Low frequency dynamics are consistent with most of the literature studied in the field of large flexible space structures. The typical control

problem that arises is that these dynamics occur at low frequencies below the controller bandwidth.

B.2. Open Loop Experimentation with the Model

The prominent dynamics of the simple model are shown to be less than 1 rad/s. Experimentation with the simple structure is conducted to understand the dynamics which would arise when trying to slew the structure. Namely, it is important to understand what inputs would excite excessive vibrations in the structure. This information is valuable to applications toward the actual plant in this investigation.

The same two types of torque inputs given to the antenna structure nominal plant are used in the open loop experimentation with this simple model. See Chapter 3 for an explanation of these inputs.

The structure model was first put under the doublet and sine wave inputs spread over time durations of 2, 4, 6, 10, 16, and 20 seconds. The time response did not show evidence of excessive vibrations from the system unless the input duration was long. Shown below are some of the time responses from the bare structure. The both types of inputs with durations of two seconds did not induce any excessive vibrations, and this was true for most of the time responses that were investigated. And this was especially true for inputs with short time durations.

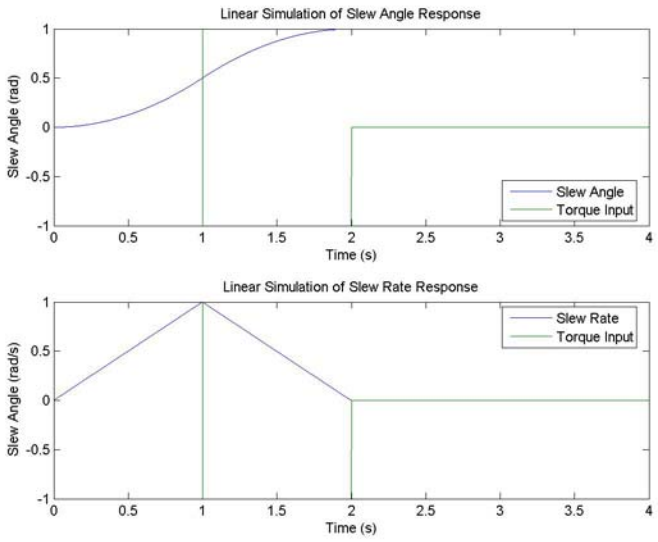

Figure B-2: Time Domain Response to a Doublet Input with a 2 Second Duration

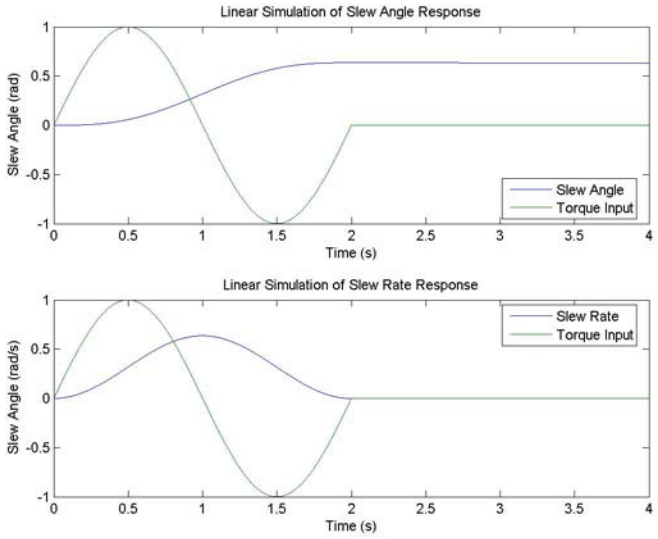

Figure B-3: Time Domain Response to a Sine Input with a 2 Second Duration

As the time durations increased, more vibration dynamics were detected. This is evident in the time response plot with a twenty second input duration. The slew rate does not return to zero as it did with the two second input. The slew rate would eventually go back to zero; however, judging from the Bode plots, the prominent dynamics indicated that this would occur over several hundred seconds after the input ended. In any case, the

final slew angle was around the area of 100 radians, which is well beyond any practical use. To slew 180 degrees (π radians), the input signal duration would be about 4.5 seconds. In this case, the vibrations could be easily damped by an integral controller.

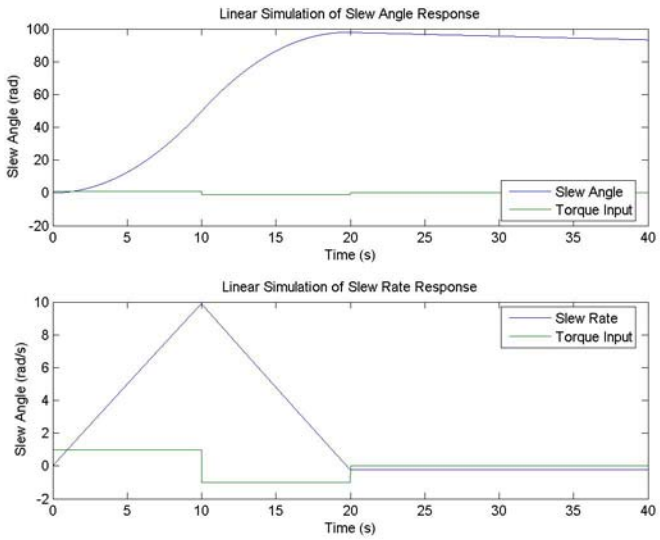

Figure B-4: Time Domain Response to a Doublet Input with a 20 Second Duration

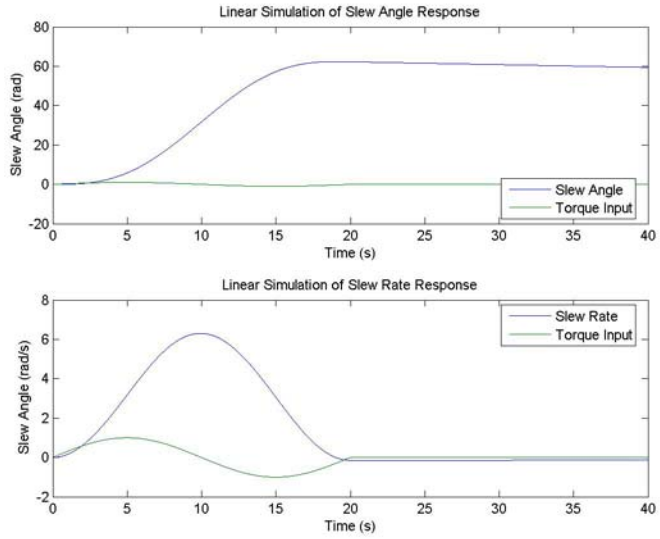

Figure B-5: Time Domain Response to a Sine Input with a 20 Second Duration

The vibrations inherent in this structure are illustrated in the next figure. From the bode plots, the most prominent dynamic response occurs at a frequency of about 3.7 x 10^{-2} rad/s. This roughly translates to a period of 170 seconds. The time response to a sine wave input with a duration of 170 seconds is shown below. The response shows prominent vibrations with little to no evidence of damping.

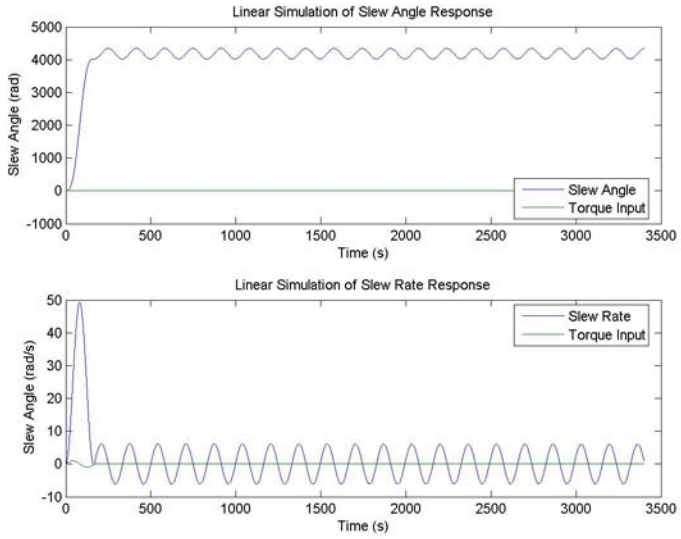

Figure B-6: Time Domain Response to a Sine Input with a 170 Second Duration

Comparing the structure frequency responses in Figure B-1 and Figure A-2, the prominent low frequency dynamics in the derived physical model are absent from the antenna structure model dynamics. It is important to note that the two models can not be directly compared to each other. The simple model relates an angle output to a torque input and the truth model relates an angle rate to a torque input. Nevertheless, the effective differences in the Bode plots are a phase shift of 90 degrees and a slope change of 20 dB per decade, thus the prominent dynamics displayed in either of the plots are still comparable.

Most of the prominent dynamics of the simple model occurred at frequencies lower than 1 rad/sec, whereas, the prominent dynamics of the truth model occurred at frequencies greater than 30 rad/sec. Also, the derived model natural frequencies were spaced far apart and the antenna plant flexible modes were spaced very close together. For these reasons, it can be concluded that the assumptions made for the simple model do not hold true for the actual antenna. However, the cause and effect principles do remain the same since the physics remain the same, and can be better viewed in a state-space model rather than in a transfer function. For this reason, the simple model is used in open loop experimentation to research desirable slewing commands, but no attempt to create a desirable feedforward controller or a feedback compensator for the simple model is considered in this investigation.

Bibliography

Alfriend, K. T., R. W. Longman, and W. S. Bercaw. "On Frequency Response Interpretation of Optimal Slewing Maneuvers, Dynamics and Control of Large Flexible Spacecraft," *Proceedings of the 2nd VPI&SU Symposium*, Blacksburg, VA. Jun 21-23, 1979. pp. 65-76.

D'Azzo, John J. and Constantine H. Houpis. *Linear Control System Analysis and Design, Conventional and Modern* (Fourth edition). New York: McGraw-Hill, 1995. pp. 580-635.

Farrenkopf, R.L., "Optimal Open-Loop Maneuver Profiles for Flexible Spacecraft." *AIAA Journal of Guidance and Control*, 2 (6): 491-498. Nov-Dec. 1979.

Junkins, J., Z. Rahman, and H.Bang. "Near-Minimum-Time Maneuvers of Flexible Vehicles: a Liapunov Control Law Design Method." *AIAA 28th Aerospace Sciences Meeting*, Reno, Nevada. Jan 8-11, 1993 (AIAA 90-0663).

Markley, F.L. "Large Angle Maneuver Strategies For Flexible Spacecraft," *AAS/AIAA Astrodynamics Specialist Conference*, June 25-27, 1979, Paper No. 79-156, pp. 625-647. (AAS 79-156)

Meirovitch, L. and R. D. Quinn. "Maneuvering and Vibration Control of Flexible Spacecraft." *The Journal of the Astronautical Sciences*, 35 (3): 301-328. July-Sep. 1987.

Schoen, Marco P., Sinchai Chinvorarat, and Gerhard M. Schoen. "Identification and Robust Control of Flexible Space Structures." *Proceedings of the American Control Conference,* 4-6 June, 2003. Vol. 6: pp. 4585-4589.

Song, Y. D. "Active Damping Control of Critical Mode Vibrations in Large Flexible Space Structures." *Proceedings of the American Control Conference*, 29 June-1 July, 1994. Vol. 3: pp. 2872-2876.

Swigert, C.J. "Shaped Torques Technique." *AIAA Conference on Large Space Platforms: Future Needs and Capabilities*, Los Angeles, CA. Sept. 27-29, 1978. (Paper No. 78-1692.)

Vita

Ensign Victor M. Barba graduated from Oxon Hill High School in Oxon Hill, Maryland. Upon his high school graduation, he enrolled in the University of Maryland in College Park, Maryland. He graduated with a Bachelor of Science Degree in Aerospace Engineering in May of 2006. He was commissioned that same month through the Navy ROTC program at The George Washington University in Washington, DC.

In June 2006, he was assigned as a student at the Graduate School of Engineering and Management, Air Force Institute of Technology at Wright-Patterson Air Force Base, Ohio. There he earned his Master of Science in Aeronautical Engineering in June 2007. Upon graduation, he will be beginning undergraduate pilot training and starting Aviation Preflight Indoctrination at Naval Air Station Pensacola.

REPORT DOCUMENTATION PAGE

Form Approved
OMB No. 074-0188

1. REPORT DATE *(DD-MM-YYYY)*	**2. REPORT TYPE**	**3. DATES COVERED** *(From – To)*
14-06-2007	Master's Thesis	June 2006 – June 2007

4. TITLE AND SUBTITLE

CONTROLLER DESIGN FOR ACCURATE ANTENNA POINTING ONBOARD A SPACECRAFT

5a. CONTRACT NUMBER

5b. GRANT NUMBER

5c. PROGRAM ELEMENT NUMBER

6. AUTHOR(S)

Barba, Victor M., ENS, USN

5d. PROJECT NUMBER
07-264

5e. TASK NUMBER

5f. WORK UNIT NUMBER

7. PERFORMING ORGANIZATION NAMES(S) AND ADDRESS(S)
Air Force Institute of Technology
Graduate School of Engineering and Management (AFIT/ENG)
2950 Hobson Way, Building 640
WPAFB OH 45433-8865

8. PERFORMING ORGANIZATION REPORT NUMBER
AFIT/GAE/ENG/07-03

9. SPONSORING/MONITORING AGENCY NAME(S) AND ADDRESS(ES)
Maj. Eric Nelson
14675 Lee Road
Chantilly, VA 20151-1715
703-808-4254

10. SPONSOR/MONITOR'S ACRONYM(S)
SECAF/ISC/T4

11. SPONSOR/MONITOR'S REPORT NUMBER(S)

12. DISTRIBUTION/AVAILABILITY STATEMENT

APPROVED FOR PUBLIC RELEASE; DISTRIBUTION UNLIMITED.

13. SUPPLEMENTARY NOTES

14. ABSTRACT

Controller design for a spacecraft mounted flexible antenna is considered. The antenna plant model has a certain degree of uncertainty. Additionally, disturbances from the host spacecraft are transmitted to the antenna and need to be attenuated. The design concept explored herein entails feedforward control to slew the antenna. Feedback control is then used to compensate for plant uncertainty and to reject the disturbance signals. A tight control loop is designed to meet performance specifications while minimizing the control gains. Simulations are conducted to show that the integration of feedforward control action and feedback compensation produces better responses than the implementation of either individual control system. Integration results in lower gains and still meets the performance specifications. Critical plant parameters are varied to simulate the uncertainty in the nominal plant. The control system is then exercised on several variations of the nominal plant. A worst case plant is produced as a combination of the variations to the nominal plant. Simulations show that when the controller is implemented on the worst case plant, specifications are exceeded. The controller gains are reduced and the simulations are repeated so that the specifications are met but not exceeded; thus, proving that a reduction of plant uncertainty allows the reduction of the control gains.

15. SUBJECT TERMS

16. SECURITY CLASSIFICATION OF:			**17. LIMITATION OF ABSTRACT**	**18. NUMBER OF PAGES**	**19a. NAME OF RESPONSIBLE PERSON**
a. REPORT	**b. ABSTRACT**	**c. THIS PAGE**			Dr. Meir Pachter
U	**U**	**U**	**UU**	98	**19b. TELEPHONE NUMBER** *(Include area code)* (937) 255-3636 x7247 (meir.pachter@afit.edu)

Standard Form 298 (Rev. 8-98)
Prescribed by ANSI Std. Z39-18